University of Nevada, Reno

Deriving Novel Allometric Equations for Northern Sierra Nevada Trees Using Terrestrial Laser Scanning

A Thesis Submitted in Partial Fulfilment of the Requirements for the Degree of Master of Science in Natural Resources & Environmental Science

By

Laura Wade

Supervised by Dr. Jonathan Greenberg/Thesis Advisor

May 2022

THE GRADUATE SCHOOL

We recommend that the thesis
prepared under our supervision by

Laura Wade

entitled

Deriving Novel Allometric Equations for Northern Sierra Nevada Trees Using Terrestiral Laser Scanning

be accepted in partial fulfillment of the
requirements for the degree of

Master of Science

Jonathan Greenberg
Advisor

Erin Hanan
Committee Member

Adam Csank
Graduate School Representative

David W. Zeh, Ph.D., Dean
Graduate School

May, 2022

Abstract

The biomass of trees is estimated by using allometric equations, which use simple tree metrics, such as diameter and height, to predict the size of the tree. Biomass is extremely important for determining carbon sequestration rates and carbon mapping in forests, as an individual tree's biomass is approximately fifty percent carbon. However, estimating the biomass of the trees is traditionally accomplished via the use of allometric equations calibrated by destructively harvesting trees in the field. Requiring destructive sampling to calibrate these models often leads to small sample sizes and a lack of a complete range of tree sizes and species sampled. An alternative solution to destructive harvesting uses terrestrial laser scanning (TLS) to estimate the volume, diameter, and height of trees in the field, and combine these with estimates of wood specific gravity. These data can then be used to generate allometric equations without many of the limitations of destructive sampling approaches. In our analysis, we scanned 108 plots located in the northern Sierra Nevada. We used TreeQSM to estimate volume for sampled trees and determined the mean species wood specific gravity to estimate biomass. We compared our QSM tree metrics against metrics measured in the field and ran a non-linear mixed effects model to determine the effect of climate on our allometric equations. Our results suggest that our two topoclimatic variables, climatic water deficit, and actual evapotranspiration, did not affect our biomass equations. We then used three allometric equation forms to estimate biomass using two different tree parameters, height, and diameter. We found that TLS can be used as a rapid method for estimating volume, height, and diameter, and we created species-specific allometric equations for trees across the Sierra Nevada that may have important applications for large-scale AGB estimation.

Acknowledgments

This research was funded by the Sierra Nevada Conservancy's Greenhouse Gas Reduction Fund for California Climate Investments, the U.S. Forest Service, and NASA's Carbon Monitoring System. This project would not have been possible without the help of GEARS lab members, including: Theo Hartsook, Adriano Matos, Taylor Brown, Katie Josifko, Dr. Adriana Parra, and Brian Mallet. In addition, this project would not have been possible without expertise from Rodney Hart, of the USFS Region 5 Remote Sensing Lab. I would like to thank my family for all their love and support through these last few years. I would also like to thank my advisor, Dr. Jonathan Greenberg, for guiding me through this project and for all the encouragement and positive feedback.

Table of Contents

List of Tables

Chapter 1

Chapter 2

List of Figures

Chapter 1

Chapter 2

List of Equations

Introduction

Of the total carbon eitted by anthropogenic sources, almost half of the anthropogenic emissions are absorbed by terrestrial and ocean sinks (Canadell et al. 2007). Since anthropogenic carbon emissions have grown faster than CO_2 sinks, identifying forests for their potential to act as carbon sinks is vital to mitigate excess anthropogenic carbon emissions (Canadell and Shultze, 2014). Carbon stock estimations rely on accurate aboveground biomass (AGB) datasets. These AGB estimates cannot be easily measured, as direct measurements of biomass traditionally required destructively sampling trees and weighing them in the field (Picard et al. 2012). Since harvesting trees and weighing them in the field is time-intensive and costly, most research uses allometric equations to estimate biomass. Forest AGB estimates typically are determined by using tree structural metrics, such as diameter-at-breast-height (DBH) and height, in allometric equations that then convert tree structure metrics into biomass and carbon estimates (Chave et al. 2005). Allometric equations are an indirect way to estimate biomass through easily measurable variables such as diameter and height (Brown et al. 1989) but destructively harvested a small number of trees to create allometric equations (Chave et al. 2005).

Allometric equations can produce large uncertainties when extrapolated to populations that have little to no data, and many allometric equations are built with relatively small sample sizes, such as a mean destructive sample size of 23 for Jenkins et al. (2003), 81 for Lambert et al. (2005) and a few hundred for Woodall et al. (2010) and Chojnacky et al. (2014). These allometric equations created with small sample sizes are often applied beyond the population they sampled from, cannot accurately represent the

biomass of a region, and thus systematically overestimate field carbon stock in North America (Duncanson et al. 2015). Duncanson et al. (2015) also suggested that allometric equation parameters vary drastically with sample size, and the error of biomass prediction when using small sample sizes may extend well above errors reported in Chave et al. (2004).

Since the limiting factor for creating accurate allometric equations historically is destructively harvesting trees, an alternative is to rely on terrestrial laser scanning (TLS) which is a very precise and easily portable LiDAR technology that can recreate forest structure to millimeter level accuracies (Disney et al. 2019). Volume can be very accurately estimated from the TLS point cloud (Raumonen et al. 2013), and when multiplied by wood specific gravity, can lead to a ± 10% uncertainty for TLS derived AGB (Calders et al. 2015). Understanding the variability of wood specific gravity across a topoclimatic gradient is crucial for predicting biomass across a region (Chave et al. 2006). The combination of region and species-specific wood specific gravity values, with increased sampling with the TLS approach, can produce novel allometric equations for the northern Sierra Nevada tree species.

References

Calders K, Newnham G, Burt A, et al (2015) Nondestructive estimates of above-ground biomass using terrestrial laser scanning. Methods Ecol Evol 6:198–208. https://doi.org/10.1111/2041-210X.12301

Canadell JG, Le Quéré C, Raupach MR, et al (2007) Contributions to accelerating atmospheric CO_2 growth from economic activity, carbon intensity, and efficiency of natural sinks. Proc Natl Acad Sci USA 104:18866–18870. https://doi.org/10.1073/pnas.0702737104

Canadell JG, Schulze ED (2014) Global potential of biospheric carbon management for climate mitigation. Nat Commun 5:5282. https://doi.org/10.1038/ncomms6282

Chave J, Andalo C, Brown S, et al (2005) Tree allometry and improved estimation of carbon stocks and balance in tropical forests. Oecologia 145:87–99. https://doi.org/10.1007/s00442-005-0100-x

Chave J, Muller-Landau HC, Baker TR, et al (2006) Regional and phylogenic variation of wood density across 2456 neotropical tree species. Ecological Applications 16:2356–2367. https://doi.org/10.1890/1051-0761(2006)016[2356:RAPVOW]2.0.CO;2

Chojnacky DC, Heath LS, Jenkins JC (2014) Updated generalized biomass equations for North American tree species. Forestry 87:129–151. https://doi.org/10.1093/forestry/cpt053

Duncanson L, Rourke O, Dubayah R (2015) Small Sample Sizes Yield Biased Allometric Equations in Temperate Forests. Sci Rep 5:17153. https://doi.org/10.1038/srep17153

Fatemi FR, Yanai RD, Hamburg SP, et al (2011) Allometric equations for young northern hardwoods: the importance of age-specific equations for estimating aboveground biomass. Can J For Res 41:881–891. https://doi.org/10.1139/x10-248

Jenkins JC, Chojnacky DC, Heath LS, Birdsey RA (2003) National-Scale Biomass Estimators for United States Tree Species. Forest Science 49:12–35

Lambert MC, Ung CH, Rauliler F (2005) Canadian national tree aboveground biomass equations. Canadian Journal for Forest Research 35:. https://doi.org/ 10.1139/X05-112

Picard N, Saint-Andre L, Henry M (2012) Manual for building tree volume and biomass allometric equations: from field measurement to prediction. FAO, Rome, Italie

Raumonen P, Kaasalainen M, Åkerblom M, et al (2013) Fast Automatic Precision Tree Models from Terrestrial Laser Scanner Data. Remote Sensing 5:491–520. https://doi.org/10.3390/rs5020491

Woodall C, Heath L, Domke G, Nichols M (2010) Methods and equations for estimating aboveground volume, biomass, and carbon for trees in the U.S. forest inventory, 2010. Gen Tech Rep. NRS-88: https://doi.org/https://doi.org/10.2737/NRS-GTR-8

Chapter 1. Variation in wood specific gravity across northern Sierra Nevada forests

Abstract

Allometric equations are widely used to predict above-ground biomass and carbon stocks in forests. These equations use easy-to-measure tree parameters, such as diameter-at-breast-height (DBH) and height. When combined with stem taper or terrestrial laser scanning (TLS) approaches to volume estimation, allometric equations require wood specific gravity as an important predictor of tree biomass. Thus, precise estimates of wood specific gravity, calculated as oven-dry mass divided by green volume, can help reduce uncertainties in allometric equations. Measurements of wood specific gravity may be particularly important in northern Sierra Nevada forests which encompass diverse temperate mixed-conifer ecosystems that will likely see a drastic shift in species composition and trait variation due to climate change and historical anthropogenic influence. To reduce biomass bias at an individual tree level, and because small sample sizes can lead to uncertainty, it is important to examine how wood specific gravity varies across a region. We calculated wood specific gravity of 329 cores across 16 different tree species in Plumas National Forest and the Lake Tahoe Basin Management Unit to understand how it varies along a climate and vegetation gradient in northern Sierra Nevada forests. Linear mixed effects models showed that most of the variation in wood specific gravity was explained by species, and, to a lesser extent, tree height, with no significant effect of climate when looking at climatic water deficit (DEF) and actual evapotranspiration (AET) as predictor variables.

1. Introduction

Forests contain approximately 45% of terrestrial carbon (Bonan, 2008) and are estimated to contain at least 522 Pg in live above-ground biomass in forests (Santoro et al. 2021). As a result, these ecosystems are responsible for approximately half of the carbon dioxide (CO_2) fluxes of all terrestrial biomes and sequestered roughly 3.5 +- 1.0 PgC yr-1 during the last 10 years (Le Quere et al. 2018). Therefore, estimating forest biomass and carbon stocks is important for understanding and modeling the global carbon cycle to offset anthropogenic carbon dioxide emissions. The global estimates of carbon stocks and sinks are uncertain (Houghton, Hall, & Goetz, 2009) and carbon stocks are typically estimated using remote sensing methods that estimate biomass over large scales (Avitabile et al. 2012). Carbon maps and sequestration rates need accurate in-situ biomass estimates; however, there can be large differences in biomass estimates especially when derived from small sample sizes (Mitchard et al. 2013). In California, landowners and land managers must develop land management strategies to improve forest health related to fire (Hurteau et al. 2011) and carbon (Swann et al. 2012).

Carbon maps at any scale using either remote sensing and/or field data rely on allometric equations relating parameters that are measured in the field, such as diameter-at-breast height and height to predict above-ground biomass and therefore individual tree stocks (Jenkins et al. 2003). Allometric equations for forested systems require trees to be destructively sampled and have been shown to be sensitive to sample size. For example, parameters for allometric equations are systematically biased relating to small sample sizes, and thus using allometric equations developed with small sample sizes may overestimate field carbon stocks in North America (Duncanson et al. 2015). Since

destructively harvesting large sample sizes is not feasible for most studies, researchers can use wood specific gravity measurements obtained through coring a tree to increase sample size and reduce biomass bias at the individual tree level (Duncanson et al. 2015). Including wood specific gravity as an important predictive variable in above-ground biomass models, in addition to diameter and height can reduce the bias of allometric models (Chave et al. 2014). However, it is important to understand the variability of wood specific gravity because ignoring the variability results in the poor predictive power of above-ground biomass equations (Baker et al. 2004).

Wood specific gravity is defined as the ratio of oven-dry mass to green volume (unitless) and is different from wood density which is defined as the mass of a wood per unit volume at a given moisture content (kg m^{-3}) and is a key functional trait of a woody plant (Williamson and Weimman, 2010). Wood specific gravity is closely tied with life-history traits and can vary with diameter, growth rate, reproduction timing, and mechanical strength of a tree and is important to plant form and function (Carlquist et al. 1977, Enquist et al. 1999). Structure determines wood specific gravity, with higher wood specific gravity trees having a greater proportion of cells with thicker cell walls (Simpson, 1993). Wood specific gravity reflects a plant's carbon investment, and is negatively associated with growth rate (Enquist et al. 1999, Muller-Landau, 2004, Wikberg & Ogren, 2004, King et al. 2005), and is positively associated with longevity and survival (Muller-Landau, 2004). Overall, long-lived, slow-growing trees tend to have a higher wood density compared to short-lived, fast-growing, pioneer species (Saldarriaga et al. 1988, Swaine & Whitmore, 1988, Wiemann & Williamson, 1988). Conventional thinking states that the fast-growing pioneer species are thought to allocate

fewer resources to strength, while slow-growing, climax species are thought to allocate more resources to greater strength. However, Larjavaara and Muller-Landau (2010) questioned whether the lower wood density of the same strength leads to high maintenance costs but lower construction costs. High wood density also provides additional benefits other than strength, including resistance to pathogens and defense against physical damage (Rowe and Speck, 2005).

Plants can respond to drought stress by increasing wood density, for example, wood density has been shown to increase with aridity (Martinez-Cabrera et al. 2009). Variation in fiber trails, specifically fiber lumen diameters which relate to cell wall thickness, is responsible for driving most of the variation in wood density (Martinez-Cabrera et al. 2009). Swenson & Enquist (2007) found a strong relationship between wood density in seed plants and variation in temperature, demonstrating key functional trait variation along an abiotic gradient. Wood density has been shown to vary across a latitudinal gradient (Wiemann & Williamson, 2002), in addition to climatic and soil nutrient gradients (Swenson & Enquinest, 2007). Wood density has been found to be responsive to drought, with density increasing with water stress as conduit wall reinforcement leads to cavitation resistance (Hacke et al. 2001). Though abiotic factors can lead to variation in wood density, the genetic component of wood density cannot be ignored. Wood density demonstrates high heritability, suggesting that abiotic forces may not be the main driver of variation in wood density at a local level (Chave et al. 2006).

The controlling factor of genetic and environmental factors on specific wood gravity is called the ‘tree effect’ and is responsible for the large inter-tree variability (Bouriaud et al. 2005). As forests are increasingly under threat from climate change,

drought stress on forest ecosystems may lead to variation in wood specific gravity, which will strongly influence the carbon storage capacity of entire forests and may be an indicator of declining ecosystem productivity. Spatial and genetic variability in wood density leads to variation in above-ground biomass calculations. Therefore, it is critical to understand wood density variation across individual, local and regional scales to reduce uncertainties in above-ground biomass estimates of a forest.

Here, we investigated the relationship between wood specific gravity and tree species, structure, and climate across a topoclimatic gradient in northern Sierra Nevada forests, California. The Sierra Nevada mixed conifer forests are increasingly vulnerable to drought stress (Van Gunst et al. 2016), overgrown forests, and frequently more common stand-replacing fires as a result of climate change, human activity, and historical fire suppression. Predicting the variability of wood specific gravity of the Sierra Nevada tree species may impact regional biomass estimates, and thus affect carbon stock estimates. We hypothesized that tree species and size would be the dominant driver of wood specific gravity variability, with wood specific gravity increasing with tree size. Further, we hypothesized that climate may play a role in influencing wood specific gravity, with wood specific gravity increasing with drought stress.

2. Methods

2.1 Area of Interest (AOI) and study species

The northern Sierra Nevada is dominated by mixed-conifer forests that are warming at a mean rate of 1 to 2.5 ° F, and the proportion of precipitation falling as rain versus snow is increasing (North et al. 2012). The climate of the Sierra Nevada is Mediterranean, with long dry summers and cool, wet winters with increasing

precipitation as elevation increases (van Mantgem & Stephenson, 2007, Guarin & Taylor, 2005). The Sierra Nevada forests start with lower elevation chaparral and woodland foothills before proceeding into ponderosa pine and mixed conifer forests. Many tree species in the Sierra Nevada are drought-tolerant, including *P. ponderosa*, *P. jeffreyii*, *Q. keloggii*, *C. decurrens*, and *J. occidentalis*.

The northern Sierra Nevada forests extend from Lake Tahoe to the southern border of Lassen National Park and across a large topoclimatic gradient and are primarily dominated by mixed-conifer forests. Within the Northern Sierra Nevada forests, we selected two primary areas of interest (AOIs) for our analysis: the Lake Tahoe Basin Management Unit (LTBMU) and Plumas National Forest. These two sites cover a wide range of the topoclimatic variability found in the Northern Sierras, covering elevations ranging from 215 to 2818 meters above sea level (Table 1).

Climate Ranges by Tree Species

Type	Scientific Name	Common name	Sample size (n)	Elevation Range (m)	Temperature Range (°C)	Annual Precipiation Range (mm)	Annual Climatic Water Deficit Range (mm)	Annual Actual Evaportanspiration Range (mm)
Angiosperm			63					
	Notholithocarpus densiflorus	Tan Oak	11	890-944	-2-27	3826-3921	13-147	451-471
	Populus balsamifera ssp. trichocarpa	Black Cottonwood	14	1472-1917	-5-25	2933-3117	140- 159	408-437
	Populus tremuloides	Quaking Aspen	26	1817-1917	-7-25	2593-2896	166-177	392-417
	Quercus kelloggii	Black Oak	12	760-1618	-4-27	3338-4051	124-177	425-461
Gymnosperm			211					
	Abies concolor	White Fir	17	1443-2334	-8-26	2786-3353	124-175	363-445
	Abies magnifica	Red Fir	32	1611-8364	-8-25	2372-3353	109-176	348-422
	Calocedrus decurrens	Incense Cedar	18	890-2019	-5-27	2932-3812	133-170	390-454
	Juniperus occidentalis	Western Juniper	9	1443-2627	-5-26	3309	168	445
	Pinus albicaulis	Whitebark Pine	6	2817	-7-24			
	Pinus contorta	Lodgepole Pine	24	1782-2334	-7-25	2372-2993	139-177	352-414
	Pinus jeffreyi	Jeffrey Pine	23	856-2222	-7-25	2766-3668	124-177	362-445
	Pinus lambertiana	Sugar Pine	19	1228-2002	-7-26	2766-3674	124-147	390-463
	Pinus monticola	Western-white Pine	16	1865-2208	-7-27	2799-2928	125-156	375-404
	Pinus ponderosa	Ponderosa Pine	20	890-1780	-7-27	2814-3668	124-188	395-438
	Pseudotsuga menziesii	Douglas Fir	17	535-1542	-5-27	3338-3916	143-177	268-272
	Tsuga mertensiana	Mountain Hemlock	10	718-2549	-9-23	2512-2748	109-139	377-381

Table 1. Climate variable minimum and maximums for each tree species, with a noticeable lack of climate data for *Pinus albicaulis* due to lack of climate data attributed to this species.

2.2 Tree selection and attribution

Plot locations were chosen as part of a larger terrestrial laser scanning (TLS) study across the northern Sierra Nevada, and our area of interest (AOI) includes 89 plots located in California's northern Sierra Nevada forests (Figure 1). To be considered, plot locations had to have more than 10% tree cover based on a LANDSAT analysis and were stratified by elevation. In addition, we excluded plot locations falling in recent burn scars or recently logged land. Plot locations were then stratified and randomly sampled according to a two-stage design to sample representative forest types in Plumas National

Forest and the Lake Tahoe Basin Management Unit. First, 10 km grid cells were placed on public lands within the boundaries of the AOIs. Secondly, two plot centers were randomly sampled from within each 10km grid cell within 60 m to 120 m of the nearest access road. This resulted in a total of 89 plots (Figure 1), including 3 opportunistic plots placed in Tahoe National Forest to sample *Juniper occidenatlis* and *Pinus monticola*, species, which needed additional plots placed due to pervasive rot (*J. occidentalis*) and rare occurrence. For each plot, we assigned all climate data (Morrison, 2018) for the period of 2019 (Table 2). Our climate dataset was downsampled from a continuous geospatial database using statistical downsampling techniques. While downsampling climate variables can incorporate fine-scale topographic features, downscaling climate data can result in worse performance for annual minima (Fowler et al. 2017).

Two water balance parameters included in these data are climatic water deficit (DEF) and actual evapotranspiration (AET), and are well-documented to control for drought stress on trees and can dictate the range where tree species occur (Stephenson, 1990, Lutz et al., 2010). DEF and AET are derived from potential evapotranspiration (PET), rain, and snow to determine available water supply, with AET= PET - DEF (Morrison, 2018). Climatic water deficit is the amount of evaporative demand that is not met by how much water is available and is an indicator of how arid a site is, while actual evapotranspiration is the evaporative water loss taken from how much water is available at a site and represents how much water is available for consumption (Stephenson, 1990). AET and DEF are well correlated with vegetation distribution compared to other climate parameters, such as temperature and precipitation (Stephenson, 1998). For this reason, we are focusing on DEF and AET as a priori variables, not only to stratify sampling across

our AOI but also as a potential indicator of variability in wood specific gravity across the climate gradient of northern Sierra Nevada forests. Plot-level topography variables, such as aspect or elevation, were not included in the correlation analysis or linear mixed effects models because the climate variables used in this study, such as water deficit (DEF), actual evapotranspiration (AET), radiation, precipitation, and snowfall were calculated using topographic predictors at a variety of scales (Morrison, 2018)

Climate Variable	Unit
Maximum Temperature (Tmax)	°C
Minimum Temperature (Tmin)	°C
Average Temperature (Tave)	°C
Actual Evapotranspiration (AET)	mm
Climatic Water Deficit (CWD)	mm
Evapotranspiration (ET0)	mm
Mean Annual Surface Radiation (RAD)	W/m^2
Annual Precipitation	mm
Annual Snow	mm

Table 2. All climate variables (Morrison, 2018) were assigned to the virtual stem maps created for each plot used in sampling.

Once the plot centers were established, we set up 30m x 30m plots, with a 5m buffer, for our field data collection. For each plot, we created stem maps within the plot by assigning tree species and DBH to each tree in the plot. In addition to the stem maps, each plot was scanned using a terrestrial laser scanning (TLS) instrument, and the resultant scan was used to create a "virtual" stem map which included the position and DBH for each tree in the plots. TLS collection, preprocessing, and virtual stem mapping are described in more detail in Hartsook (2021). These virtual stem maps were linked

with the field-collected stem maps, as well as the plot-level topoclimate data to create a final stem map that contained the position, species, DBH, and local topoclimate of each tree in the plots, for N= 5,873 trees mapped.

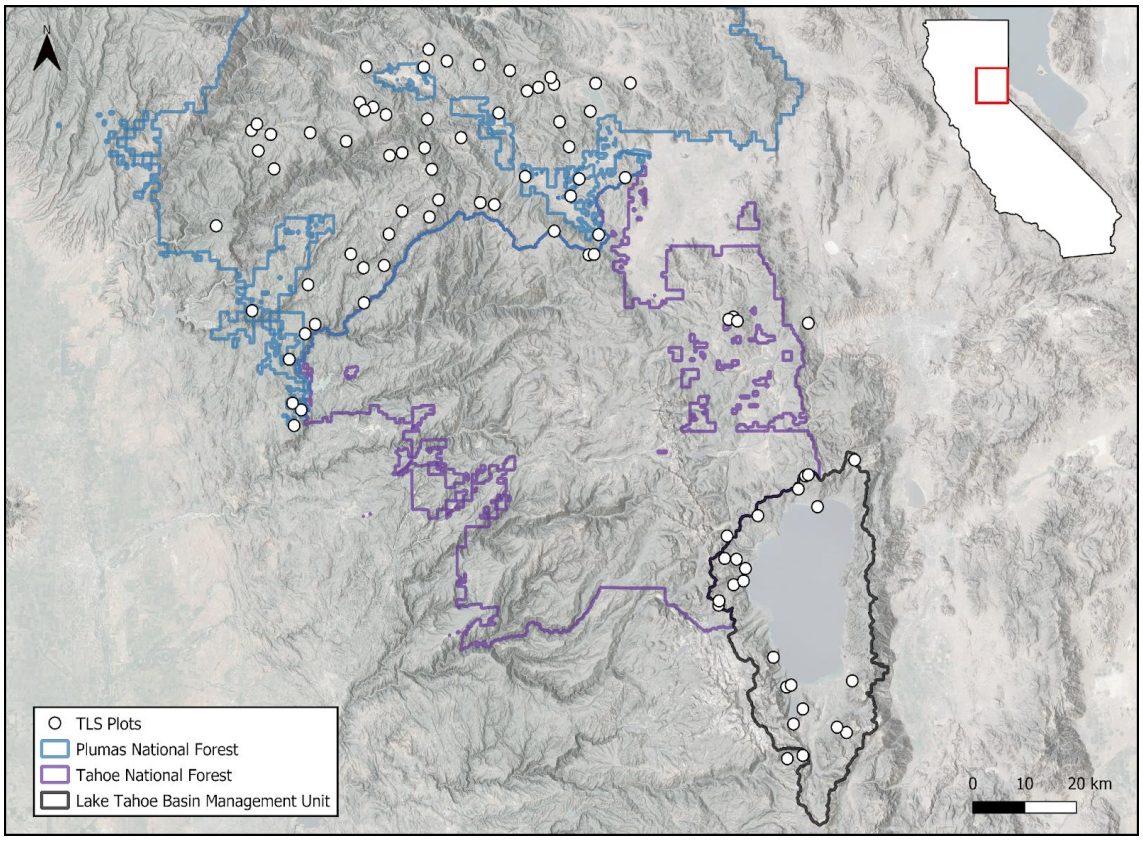

Figure 1. TLS plot locations (n=89) across Plumas National Forest and Lake Tahoe Basin Management unit, with three opportunist plots placed in Tahoe National Forest to sample *J. occidenatalis and P. monticola*. We included one plot located in Nevada (located in the Mt. Rose Wilderness) to sample *P. albicaulis*.

From our tree database, we performed stratified sampling to select trees we planned to take wood specific gravity measurements from, to try to sample as evenly as possible across the multivariate stratification space. We stratified across tree species, diameter size class, and climatic water deficit (DEF). We determined each species' climatic water deficit range and sampled evenly across CWD in 25 mm bins ranging from 50 mm to 200 mm. Within each CWD bin, we sampled across DBH ranging from 15 cm

to 130 cm in 10 cm bins. In total, 329 trees were selected across 16 tree species and 12 size classes. Figure 2 shows the sample sizes for each of these bins. The range of DBH size classes sampled extended from 15 cm to 130 cm with the goal of sampling evenly across all DBH size classes for each tree species. Figure 2 illustrates that just under half of our total number of samples were collected in the 15-25 and 25-35 cm DBH size classes; this is due to many of the smaller diameter trees, including *Populus tremuloides, Quercus kelloggii*, *Notholithocarpus densiflorus*, do not get very large even as adult trees. In addition to coring, we collected tree measurements (329 in total) in the field, including DBH (diameter-at-breast height) using a DBH tape, tree height, crown spread, and lowest live crown using standard forest mensuration equipment and techniques (National Core Field Guide, 2019) using a laser rangefinder (TruPulse 360 Laser Rangefinder).

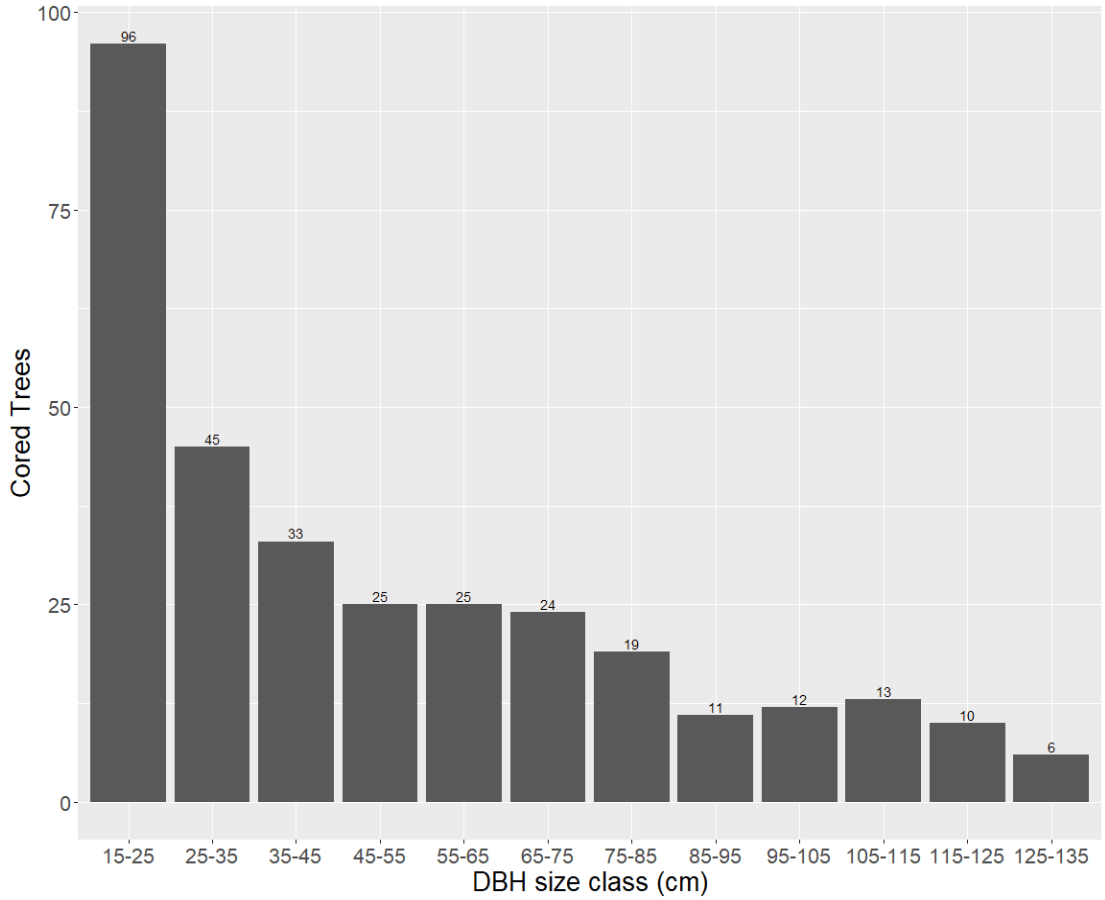

Figure 2. Sample sizes of cored trees to obtain wood specific gravity measurements for each 10 cm DBH bin ranging from 15cm to 135 cm. The 15-25 and 25-35cm range consisted of a majority of cored trees because some tree species, for example, *P. tremuloides, Q. kelloggii, N. densiflorus,* are smaller in diameter compared to mixed conifer species that become large, late-successional tree species.

Climate variables were calculated at a plot level to test the variability of wood specific gravity with climate across a tree species range in the northern Sierra Nevada forests. We ran a Pearson correlation test on all the climate variables (DEF, AET, ET0, T_{min}, T_{max}, T_{ave}, RAD, rain, and snow) to evaluate potential climate predictor variables and selected uncorrelated variables ($r < 0.65$) with variance inflation factors less than 5 from the "car" package (Weisberg, 2019) to check for multicollinearity. Refer to Table 3 to see which pairs of variables are highly correlated (> 0.65) and which variables were

selected randomly from each of the correlated pairs. The final set of predictor variables, after removing correlated pairs, included tree species, height, DEF, and AET, and these variables were used in subsequent linear mixed effects models (Table 3). In Figure 4, we illustrated the predictor variables and their proxy variables, with tree height as a proxy for diameter and linked tree size to WSG variation, while DEF and AET were proxies for temperature (T_{min}, T_{max}, T_{ave}) and precipitation and snowfall variables (annual rain and snow) and demonstrated the link of water availability (or drought stress) to WSG Variation (Table 3).

2.3 Field sampling and sample processing

We located our target trees identified in our sample design during a subsequent site visit. For each selected tree we assessed the tree for signs of disturbance such as insect damage or disease, and only 'healthy' trees were ultimately cored and measured. Each target tree was cored using a 5.15mm wide increment borer at DBH until it reached the pith and all extracted cores were stored in a dry place. If rot was found in the tree, the core was discarded and the target tree was either cored again from a different direction, or a new tree was chosen of the same species and DBH bin. No trees were cored more than twice to ensure that the tree could survive sampling.

For each core, we measured the basic wood specific gravity (WSG_b) as the ratio of oven-dried mass to green volume (WSG_b =oven dry mass/ green volume / ρ water) (Chave et al. 2006). Each core was defined as a pith-to-bark sample with both pith and bark removed, and samples were oven-dried for 48 to 72 hours in a well-ventilated oven at 103 ° C until mass was constant. After the core was dried, we weighed each sample to the precision of 0.01 g before calculating the green volume by the water displacement

method (Ilic et al. 2000). The water displacement method provides more reliable estimates than the caliper method for calculating the volume of regular and irregular-shaped samples (Chave et al. 2006). A beaker was filled with deionized water and each core sample was forced underwater with a small pin, with careful attention paid to each core not touching the sides or bottom of the beaker. The measured mass of the displaced water is equal to the green volume of the sample.

Hardwoods exhibited a much higher mean WSG (0.72 for *Quercus kellogii* and 0.66 for *Notholithocarpus densiflorus)* compared to the softwood *Pinus, Abies,* and *Populus* sp. (*P. blsamifera* spp.) (Figure 3, Table 2). There was substantial WSG variability not only across tree species but great variation within each tree species, with values ranging as much as 0.3 for *Tsuga mertensiana* (Table 2).

2.4 Analysis

Our goal was to test for the effect and direction of climate, species, and structure on wood specific gravity. Our full list of potential predictor variables is described in Table 3. Before we began our analysis, we ran a Pearson correlation test on all variables (DBH, Height, DEF, AET, ET0, T_{min}, T_{max}, T_{ave}, RAD, rain, and snow) to evaluate potential predictor variables and selected uncorrelated variables ($r < 0.65$) with variance inflation factors less than 5 from the "car" package (Weisberg, 2019) to check for multicollinearity. Refer to Table 3 to see which pairs of variables are highly correlated (> 0.65) and which variables were selected randomly from each of the correlated pairs. The final set of predictor variables, after removing correlated pairs, included tree species, height, DEF, and AET, and these variables were used in subsequent linear mixed effects models (Table 4). Plot ID was included in this analysis to account for the random effect

that plot locations contribute, as the plot locations are only a small subset of the region we want to make an inference for.

Predictor Variable	Link to WSG Variation	Correlated Variables	Description
Tree Species			
Height	Tree size		Tree height in meters
		Diameter	Tree diameter at 1.37 m in centimeters
Climatic Water Deficit (DEF)	Climate stress		Water balance metric at a plot level in milimeters; amount of evaporative demand that is not met by available water
Actual Annual Evaopotranspiration (AET)	Climate stress		Water balance metric at a plot level in milimeters; Evaporative water loss of available water for consumption
		Annual Snow	Annual snow (mm)
		Annual Precipiation	Annual precipitation (mm)
		Minimum Temperature	Mean temperature of the coldest month (°C)
		Maximum Tempearture	Mean temperature of the warmest month (°C)
		Average Temperature	Mean annual temperature (°C)
		Radiation	Mean Annual short-wave downelling surface radiation (W/m^2)

Table 3. Candidate predicted variables randomly chosen from each correlated pair and their associated proxy variable. Methods for deriving these climate variables calculated for each plot are described in Morrison et al. 2018.

To assess trends in wood specific gravity as a function of our predictor variables, we used linear mixed effects models via the "lmer" function from the "lme4" package (Bates et al. 2015) in R version 4.1.1 (R Core Team, 2021). Wood specific gravity was tested on the pared-down set of predictor variables (Table 3) and plot ID was included in each model as a random effect to account for any variation, as the plot locations are only a small subset of AOI about which we want to make an inference. We compared scaling the predictor variables and decided to use unscaled variables to ensure ease of interpretation, and scaling did not produce any. We used "dredge" in the "MuMIn" package in R (Barton, 2020) that performs model selection using every combination of

our chosen predictor variables and ranks the best fitting models according to the lowest Akaike's Information Criterion corrected for small sample sizes (AIC_c) score which prefers simpler models with fewer parameters if the change in AIC_c (ΔAIC_c) <2 (Burnham & Anderson, 2002). Since ΔAIC_c was <2 for the top models returned in by the "dredge" function, a model averaging approach ("model.avg" function in the "MuMin" package) was used with the top four models with a ΔAIC_c <2. Model averaging ranks selected models and uses estimates for each candidate model and their respective weights and can provide a robust set of parameter estimates (Burnham & Anderson, 2002) before averaging these across multiple models to avoid the issue of picking one model with a ΔAIC_c <2. The goal of model averaging is to use Akaike weights for predictor variables that are on the same scale and to incorporate models with similar support in the data. The outputs of the model average are the parameter estimates of 4 different models and we interpreted the 'conditional' subset coefficients of the averaged model. Parameter estimates (β), p-values, and Pseudo-R^2 values were calculated (Table 5) along with the effect sizes of each predictor variable for the averaged model (Figure 4). Pseudo-R^2 values were produced using the "r.squaredGLMM" function in the "MuMIn" Package (Barton, 2015).

3. Results

3.1 Linear mixed effects model results

For each tree species, we calculated mean, variance, and standard deviation of the WSG values (Figure 3). The distribution of wood specific gravity ranged greatly for some species (0.3 for *T. mertensiana)* and ranged little for other species (0.1 for *P. lambertiana*). *Q. kelloggi* experienced the highest WSG with a mean of 0.72 +-.072 while

P. balsamifera spp. trichocarpa experienced the lowest WSG with a mean of 0.39 +- 0.041 (Table 4). Hardwood species exhibited a much higher mean WSG (0.72 for *Quercus kellogii* and 0.66 for *Notholithocarpus densiflorus)* compared to the softwood species (Figure 3). There was substantial WSG variability not only across tree species but variation within each tree species, with values ranging as much as 0.3 for *Tsuga mertensiana* (Table 4).

Scientific Name	Scientific.Name	Common name	Mean WSG	Standard Deviation of WSG	Diameter Range (cm)	Height Range (m)	Miles et al. (2009) Mean WSG
Abies concolor	Abies concolor	White Fir	0.439	0.050	16.5-131.3	3.8-58.6	0.37
Abies magnifica	Abies magnifica	Red Fir	0.481	0.066	10.0-155.4	7.8-52.7	0.36
Calocedrus decurrens	Calocedrus decurrens	Incense Cedar	0.398	0.066	12.0-124.7	8.9-34.2	0.35
Juniperus occidentalis	Juniperus occidentalis	Western Juniper	0.471	0.075	22.4-75.6	7.8-13.7	0.45
Notholithocarpus densiflorus	Notholithocarpus densiflorus	Tan Oak	0.661	0.047	13.0-34.4	11.8-24.4	0.58
Pinus albicaulis	Pinus albicaulis	Whitebark Pine	0.516	0.070	13-39.3	1.8-13.5	0.43
Pinus contorta	Pinus contorta	Lodgepole Pine	0.499	0.056	7.5-83.7	8.7-34.6	0.38
Pinus jeffreyi	Pinus jeffreyi	Jeffrey Pine	0.495	0.044	19.6-124.1	7.5-46.9	0.37
Pinus lambertiana	Pinus lambertiana	Sugar Pine	0.416	0.029	13.8-151.8	8.5-54.9	0.34
Pinus monticola	Pinus monticola	Western-white Pine	0.468	0.055	30.1-81.2	7.7-47.5	0.36
Pinus ponderosa	Pinus ponderosa	Ponderosa Pine	0.537	0.073	13.3-100.3	8.3-52.7	0.38
Populus balsamifera ssp. trichocarpa	Populus balsamifera ssp. trichocarpa	Black Cottonwood	0.391	0.041	17.2-119.5	7.9-36.8	0.31
Populus tremuloides	Populus tremuloides	Quaking Aspen	0.478	0.061	10-29.3	9.3-20.2	0.35
Pseudotsuga menziesii	Pseudotsuga menziesii	Douglas Fir	0.559	0.053	11.4-118	7.3-48.8	0.45
Quercus kelloggii	Quercus kelloggii	Black Oak	0.716	0.072	14.9-52.5	6.4-28.9	0.51
Tsuga mertensiana	Tsuga mertensiana	Mountain Hemlock	0.586	0.111	12.9-71.6	3.8-30.5	0.42

Table 4. Wood specific gravity means, standard deviation, range and variance, and diameter and height range across tree species. Means of WSG can be compared to Miles and Smith (2009) wood specific gravity values (green volume and oven dry mass) for trees of North America.

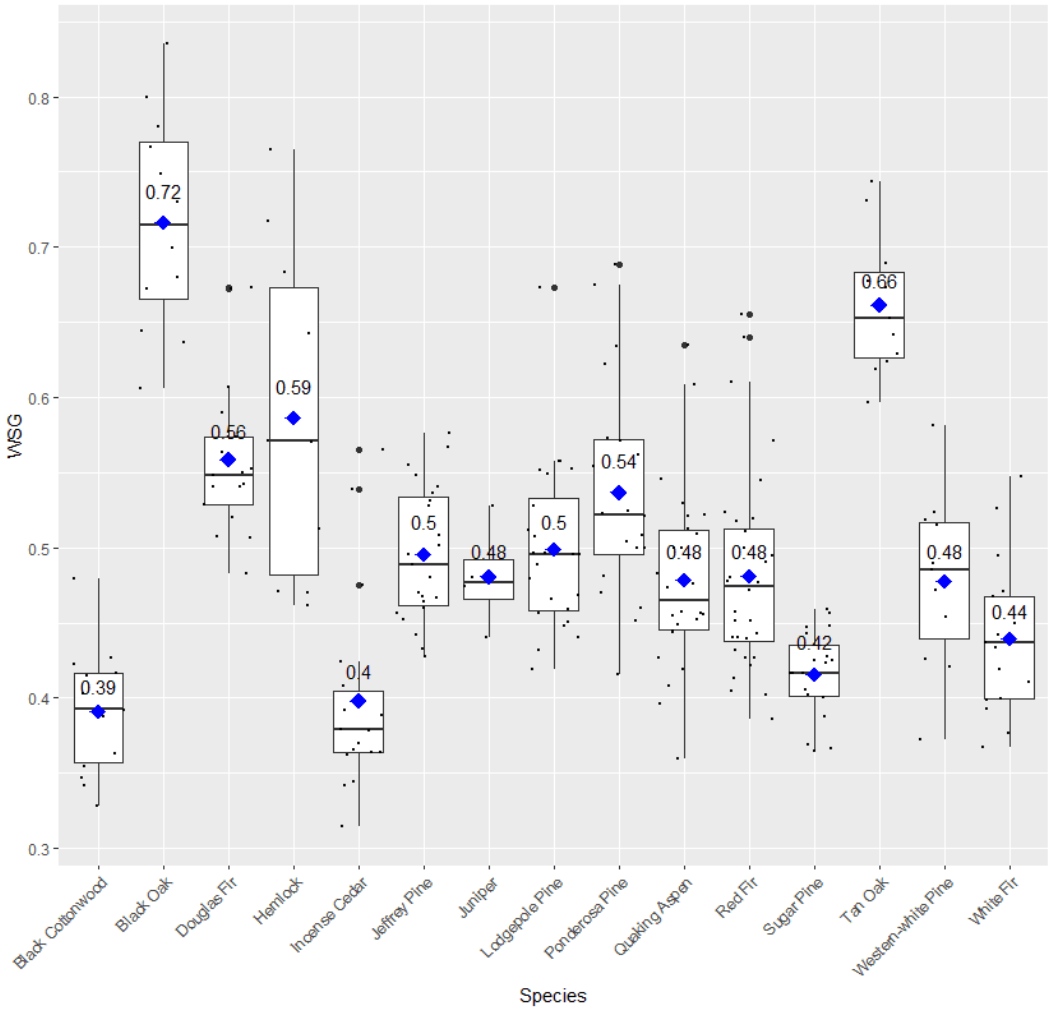

Figure 3. Mean and range of WSG values for each tree species sampled, with means (blue diamond symbol) with a 'jitter' effect demonstrating sample size for each species. Boxplot with jitter conducted in the "ggplot2" package (Wickham, 2016).

We tested the relationship of 329 wood specific gravity values with tree species, tree size, and climate with linear mixed effects models. Model averaging of our full linear mixed effect model returned four top models with a delta $AIC_c < 2$ (Table 5). Not wanting to rely purely on the AIC_c score, we also looked at estimated regression coefficients (β) and the marginal and conditional R^2 values, which return the explained variance of fixed effects (and random effects) in the model and can be used to determine

the fit of a model (Harrison et al., 2018). Wood specific gravity was best explained by species in the average LMM with significant p values <0.001 for all species except for *Pinus lambertiana* and *Calocedrus decurrens* (Table 5). The high marginal and conditional R^2 values, ranging from 0.66 to 0.65, for all the LMMs (Table 5) indicates a high percentage of variance in the response variable (WSG) explained collectively by the predictor variables. However, high R^2 values are not necessarily a true indicator of goodness of fit, so we evaluated these data, which had approximately normal distributions and were modeled using the default "Gaussian" family. The residuals for each model were approximately normal and we proceeded in using R^2 values to explain the variation each model explains. The random effect variance of "plot" for all 5 models was between 2.16e-12 and 2.4e-12 which is very small but we still included it in our models as a random effect. The effect sizes of the linear mixed effects models indicated that tree species accounted for the majority of the variation in WSG, along with height; however, water balance variables (DEF and AET) did not have an effect on our response variable were not significant (Figure 4). Partial effect plots for our LMMs suggest that while WSG was best explained by species, climate effects had a negligible effect across the range of plots and species sampled (Figure 5). Tree height significantly accounted for variation in wood specific gravity in the averaged LMM model with an estimated regression coefficient (β) of -8e04 and a p-value < 0.05 (Table 5), suggesting that overall wood specific gravity decreases with tree size. Our results highlight the strong influence of tree species, and to a lesser extent, tree size, on WSG variation, with climate stressors not playing a significant role in the linear mixed effect models (Table 3). When looking

at individual species' WSG response to tree height and climate (Figure 6), we found no consistent pattern relating tree size, DEF, or AET with WSG variation across tree species.

Model	Predictors	ß	P	AICc	Marginal R2	Conditional R2
Model 1	Intercept	0.39	**<0.0001**	-706.6	0.66	0.66
	Species	1.6				
	Height	-0.01	**0.01275**			
	DEF	-0.007	0.11			
Model 2	Intercept		**<0.0001**	-706.3	0.66	0.66
	Species	1.8				
	Height	-0.01	**0.011**			
	AET	0.008	0.14			
Model 3	Intercept	0.39	**<0.0001**	-706.1	0.66	0.66
	Species	1.76				
	Height	-0.011	**0.008**			
	DEF	-0.006	0.17			
	AET	0.007	0.21			
Model 4	Intercept	0.39	**<0.0001**	-706.1	0.65	0.65
	Species	1.7				
	Height	-0.01	**0.02**			
Averaged (conditional) Model	Intercept	0.39	**<0.0001**		0.66	0.66
	Species	1.74				
	Height	-8e-04	**0.017**			
	DEF	-4e-04	0.15			
	AET	3e-04	0.18			

Table 5. Estimated regression coefficients from 5 LMM models (β, p-value, AIC_c, Marginal R^2 and Conditional R^2) predicting wood specific gravity values. Variables included in the full model were climatic water deficit (DEF), actual evapotranspiration(AET), species and height. We used Akaike's Information Criterion corrected for small sample sizes (AIC_c) which prefers simpler models with fewer parameters if the change in AIC (ΔAIC_c) <2. Larger ΔAIC_c values indicate that the model with the lowest AIC value is the best fit model (Brunham and Anderson, 2002). Bolded p-values are significant ($P < 0.05$), while p-values of non-significant predictors retained

in the models are not bolded. The random effect variance for all models was between 2.16e-12 and 2.4e-12.

Figure 4. Effect sizes for the average linear mixed-effects model with species responsible for the majority of the variation in WSG. The blue illustrates a positive effect size, with WSG increasing with the predictor variable, and red shows a negative effect size, with WSG decreasing with the predictor variable. DEf and AET are not significant while tree species and, to a lesser extent, tree size explained most of the variability in WSG.

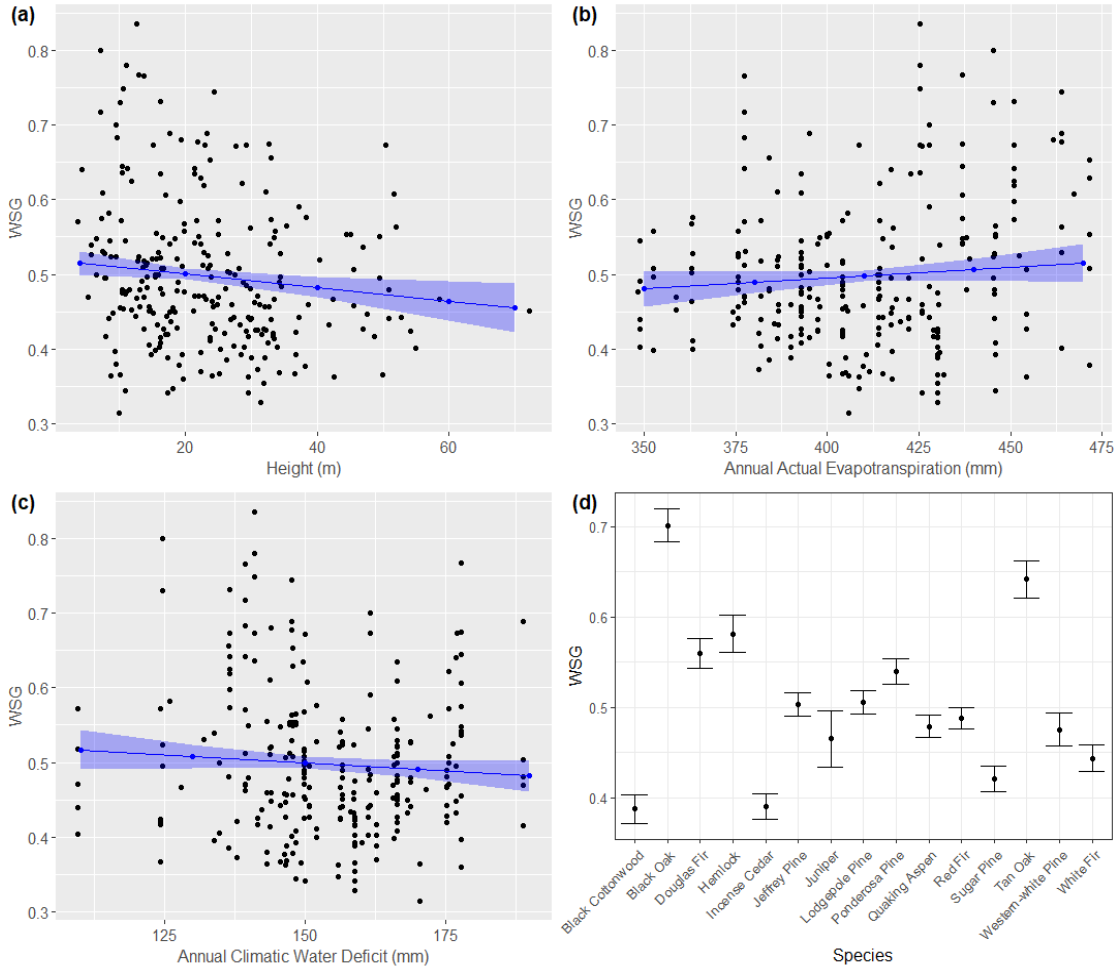

Figure 5: Partial effect plots from the linear mixed-effects model predict wood specific gravity variation as a function of **a)** Height (m), **b)** Actual Evapotranspiration (AET), **c)** climatic water deficit (DEF) and **d)** tree species. All models included a random intercept of plot ID. The shaded blue areas represent a 95% confidence interval.

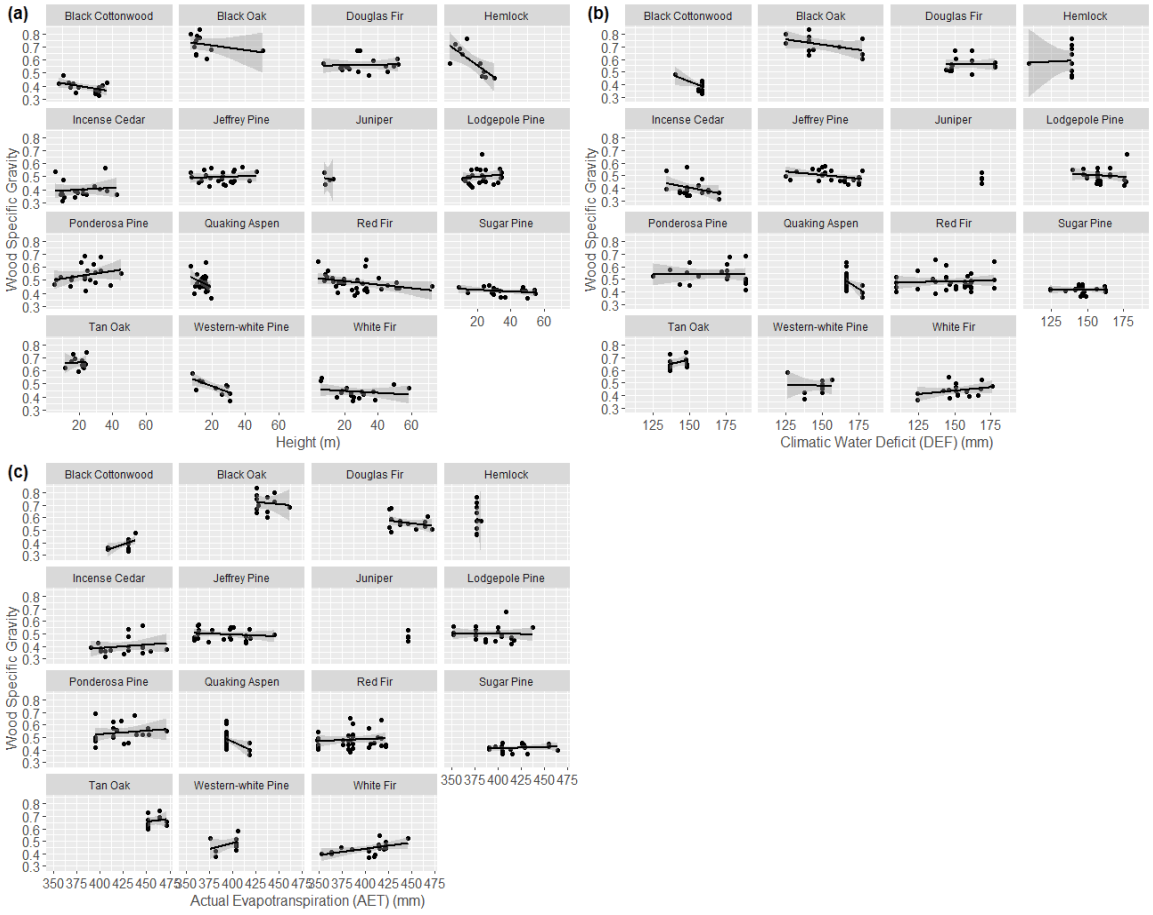

Figure 6. Tree size and drought stressors linked to variation of wood specific gravity across tree species by **a)** height, **b)** climatic water deficit, and **c)** actual annual evapotranspiration.

4. Discussion

The aim of our study was to examine what factors influence the variability in WSG across northern Sierra Nevada trees, with the ultimate goal of how this understanding can potentially reduce uncertainties in carbon estimates of trees. We found that species was the primary factor driving variability in WSG, confirming that species are responsible for a high degree of variability in WSG (Fimbel and Sjaastad, 1994, Jordan et al. 2008, Phillips et al. 2019). However, within species, we did find that the height of the tree contributed to the overall WSG estimates, with taller trees showing

lower wood specific gravity than shorter trees. Finally, across species, we also found a small impact of topoclimate, with wood density decreasing with increasing climatic water deficit (CWD) and with decreasing actual evapotranspiration (AET). Since wood specific gravity has been known to vary with tree size, species, and climate, and biomass estimates rely on wood specific gravity, the variance of wood specific gravity across the northern Sierra Nevada will have important implications on forest ecology, management, and carbon estimates for each species.

4.1 Species influence

Our results demonstrate the pervasiveness of species-driven variation in wood specific gravity. Variation in wood specific gravity among species can be explained by life-history traits in addition to genetic variation among tree species (Muller-Landau, 2004). Our dataset encompasses tree species with low WSG, such as *P. balsamifera* ssp. *trichocarpa* and *C. decurrens* and species with high WSG, such as *Q. kelloggii* and *N. densiflorus*. Oak species, such as *Q. Kelloggii* and *N. densiflorus*, are hardwood trees that exist in lower elevation forests in the northern Sierra Nevada which typically are under drought conditions and have a higher wood density compared to the higher elevation tree species that receive more precipitation. Riparian tree species, such as black cottonwood (*P. balsamifera ssp. trichocarpa*) and quaking aspen (*P. tremuloides*) tend to have a lower wood specific gravity due to the high availability of water, while incense cedar (*C. decurrens*) is a slow-growing species that is typically tolerant to drought, but has a lower wood specific gravity mean compared to other drought-resistant conifers in our dataset. The drought-resistant conifers in our dataset (*P. jeffreyii, P. ponderosa, J. occidentalis, and C. decurrens*) display higher wood specific values compared to published mean

wood specific gravities for North American trees (Miles and Smith, 2009), which could reflect a strategy for drought-resistant conifers increasing wood specific gravity by increasing latewood tracheid widths as a response to drought (Bjorklund et al. 2017). Softwood conifer species (*Abies* sp. and *Pinus* sp.) make up the middle range of wood specific gravity values and have a lower WSG value than the hardwoods. It is important to acknowledge that when we describe species as the primary factor of predicting variability of WSG, we are also describing climate, as climate, and in particularly, aridity, predicts species' distributions (Stephenson, 1998). Increasing our level of understanding of species-level WSG variability will more accurately determine stand-level biomass, and thus carbon estimates.

4.2 Size influence

Although species explains most of the variance of these data, tree size also plays a significant role, with taller trees having a lower specific gravity compared to shorter trees across tree species, which provides support that functional traits, such as wood specific gravity, can be associated with different life-history strategies. Our results highlight conventional thinking, with taller trees reflecting the fast-growing, early-successional life-history traits that have lower specific gravity woods, and shorter trees reflecting the slow-growing, late-successional life-history trait with higher wood specific gravity and lower background mortality rates (Chave et al. 2009). Thus, strength and construction cost linearly increase with wood specific gravity, with pioneers having lower wood specific gravity (vanGelder, Poorter & Sterck, 2006, Larjavaara & Muller-Landau, 2010). However, there are a lot of inter-specific variability, as some tree species, such as *T. mertensiana* and *P. monticola* show a sharp decrease of wood specific gravity with height

that follows with conventional thinking, while other tree species, such as *P. jeffreyi*, *P. ponderosa*, and *C. decurrens*, which are drought-tolerant conifers, demonstrate a slight increase of wood specific gravity with tall trees. This can be explained by inter-tree variability, as life-history traits, soil fertility, genetic heritability, and stand characteristics can also influence WSG variability, not just tree size.

4.3 Climatic influence

Northern Sierra Nevada's mixed conifer forests' persistence under climate change will depend on tree species' ability to cope with drought stress. It is reported that trees with denser wood are more able to retain water under drought conditions and have lower mortality rates during drought (Nardini et al. 2013, Greenwood et al. 2017). Contrary to our expectations, climate does not explain regional variation in wood specific gravity, and we did not see the effect of drought stress on WSG. Although wood specific gravity slightly increased with climatic water deficit (DEF) and slightly decreased with increased actual evapotranspiration (AET), climate was not a factor for WSG variation when looking at the effect on all species. The lack of significance of climate on WSG variability may indicate that climate may not play a role in influencing wood specific gravity across the northern Sierra Nevada, especially for tree species that are already existing under drought conditions for many years. Other studies that found no association between climate and wood specific gravity distribution include Ter Steege and Hammond (2001), which saw a lack of significance in tree-level wood specific gravity and rainfall in Guyana, while Williamson (1984) found a lack of significance in the wood densities of wetter versus drier sites in Costa Rica. The lack of strong influence of climate on our data may be explained from other numerous other factors, such as genetic heritability, growth

rate, soil fertility, and competition (Muller-Landau et al. 2004, Hacke et al. 2015, Kunstler et al. 2016). In addition, variation in disturbances, such as stand-replacing fires, may be more important in future determinations of wood specific gravity variation. Further studies elucidating the relationships between species, tree size, life-history traits, climate, and disturbance may reveal in more detail the patterns of wood specific gravity over a region. In addition, future research can pull apart moisture limitations for each season, such as seasonal precipitation, which can be associated with variation in wood specific gravity for some coniferous trees (Carrillo et al. 2016).

4.4 Conclusions

These results show that wood specific gravity is correlated with species and tree height but does not vary significantly across the topoclimatic gradient of the northern Sierra Nevada. Accounting for variation of wood specific gravity means across a large region can improve biomass estimates. Our results for this study provide insights into wood specific gravity variation among tree species in the northern Sierra Nevada, which dictates carbon storage estimates and carbon sequestration rates for trees. Managing forests for carbon storage and sequestration is a priority with climate change promoting an increased fire hazard, overcrowding, and drought stress to forests, and understanding the variability of wood specific gravity of tree species in the northern Sierra Nevada forests will help managers predict volume, biomass, and carbon inventories for the region.

5. References

Avitabile V, Herold M, Heuvelink GBM, et al (2016) An integrated pan-tropical biomass map using multiple reference datasets. Glob Change Biol 22:1406–1420. https://doi.org/10.1111/gcb.13139

Baker TR, Phillips OL, Malhi Y, et al (2004) Variation in wood density determines spatial patterns inAmazonian forest biomass: Wood specific gravity and Amazonian biomass estimates. Global Change Biology 10:545–562. https://doi.org/10.1111/j.1365-2486.2004.00751.x

Bates D, Mächler M, Bolker B, Walker S (2015) Fitting Linear Mixed-Effects Models Using lme4. J Stat Soft 67:. https://doi.org/10.18637/jss.v067.i01

Barton, K. (2020) Mu-MIn: Multi-model inference. R Package Version 0.12.2/r18. http://R-Forge.R-project.org/projects/mumin/

Björklund J, Seftigen K, Fonti P, et al (2020) Dendroclimatic potential of dendroanatomy in temperature-sensitive Pinus sylvestris. Dendrochronologia 60:125673. https://doi.org/10.1016/j.dendro.2020.125673

Bonan GB (2008) Forests and Climate Change: Forcings, Feedbacks, and the Climate Benefits of Forests. Science 320:1444–1449. https://doi.org/10.1126/science.1155121

Bouriaud O, Leban J-M, Bert D, Deleuze C (2005) Intra-annual variations in climate influence growth and wood density of Norway spruce. Tree Physiology 25:651–660. https://doi.org/10.1093/treephys/25.6.651

Burnham KP, Anderson DR (2004) Multimodel Inference: Understanding AIC and BIC in Model Selection. Sociological Methods & Research 33:261–304. https://doi.org/10.1177/0049124104268644

Carlquist SJ (1975) Ecological strategies of xylem evolution. University of California Press, Berkeley

Carrillo-Varela I, Aguayo MG, Valenzuela S, Teixeria Mendonca R (2015) Variations in wood anatomy and fiber biometry of Eucalyptus globulus genotypes with different wood density. Wood Research 60:1–10

Chave J, Muller-Landau HC, Baker TR, et al (2006) Regional and phylogenic variation of wood density across 2456 neotropical tree species. Ecological Applications 16:2356–2367. https://doi.org/10.1890/1051-0761(2006)016[2356:RAPVOW]2.0.CO;2

Chave J, Réjou-Méchain M, Búrquez A, et al (2014) Improved allometric models to estimate the aboveground biomass of tropical trees. Glob Change Biol 20:3177–3190. https://doi.org/10.1111/gcb.12629

Duncanson L, Huang W, Johnson K, et al (2017) Implications of allometric model selection for county-level biomass mapping. Carbon Balance Manage 12:18. https://doi.org/10.1186/s13021-017-0086-9

Enquist BJ, West GB, Charnov EL, Brown JH (1999) Allometric scaling of production and life-history variation in vascular plants. Nature 401:907–911. https://doi.org/10.1038/44819

Fox J, Weisberg S (2019). *An R Companion to Applied Regression*, Third edition. Sage, Thousand Oaks CA. https://socialsciences.mcmaster.ca/jfox/Books/Companion/.

Greenwood S, Ruiz-Benito P, Martínez-Vilalta J, et al (2017) Tree mortality across biomes is promoted by drought intensity, lower wood density and higher specific leaf area. Ecol Lett 20:539–553. https://doi.org/10.1111/ele.12748

Guarín A, Taylor AH (2005) Drought triggered tree mortality in mixed conifer forests in Yosemite National Park, California, USA. Forest Ecology and Management 218:229–244. https://doi.org/10.1016/j.foreco.2005.07.014

Hacke UG, Sperry JS, Pockman WT, et al (2001) Trends in wood density and structure are linked to prevention of xylem implosion by negative pressure. Oecologia 126:457–461. https://doi.org/10.1007/s004420100628

Harrison XA, Donaldson L, Correa-Cano ME, et al (2018) A brief introduction to mixed effects modelling and multi-model inference in ecology. PeerJ 6:e4794. https://doi.org/10.7717/peerj.4794

Hartsook T (2021) Discovetree - An Automated Tool To Generate Stem Maps From Terrestrial Laser Scanner Point Clouds. University of Nevada, Reno

Houghton RA, Hall F, Goetz SJ (2009) Importance of biomass in the global carbon cycle: Biomass in the global carbon cycle. J Geophys Res 114:n/a-n/a. https://doi.org/10.1029/2009JG000935

Hurteau MD, Stoddard MT, Fulé PZ (2011) The carbon costs of mitigating high-severity wildfire in southwestern ponderosa pine: Carbon costs of mitigating wildfire. Global Change Biology 17:1516–1521. https://doi.org/10.1111/j.1365-2486.2010.02295.x

Ilic, J., D. Boland, M. Mcdonald, G. Downes and P. Blakemore, 2000. Wood density phase 1: State of knowledge, national carbon accounting system. Australian Greenhouse Office, Commonwealth of Australia. Technical Report No. 18.

Jenkins JC, Chojnacky DC, Heath LS, Birdsey RA (2003) National scale biomass estimators for United States tree species. Forest Science 49:

Jordan L, Clark A, Schimleck LR, et al (2008) Regional variation in wood specific gravity of planted loblolly pine in the United States. Can J For Res 38:698–710. https://doi.org/10.1139/X07-158

King DA, Davies SJ, Supardi MNN, Tan S (2005) Tree growth is related to light interception and wood density in two mixed dipterocarp forests of Malaysia. Funct Ecology 19:445–453. https://doi.org/10.1111/j.1365-2435.2005.00982.x

Kunstler G, Falster D, Coomes DA, et al (2016) Plant functional traits have globally consistent effects on competition. Nature 529:204–207. https://doi.org/10.1038/nature16476

Larjavaara M, Muller-Landau HC (2010) PERSPECTIVE: Rethinking the value of high wood density: Rethinking the value of high wood density. Functional Ecology 24:701–705. https://doi.org/10.1111/j.1365-2435.2010.01698.x

Le Quere C, Andrew RM, Friedlingstein P, et al (2018) Global Carbon Budget 2018. Earth System Science DAta 10:2141–2194. https://doi.org/https://doi.org/10.5194/essd-10-2141-2018

Lutz JA, van Wagtendonk JW, Franklin JF (2010) Climatic water deficit, tree species ranges, and climate change in Yosemite National Park. Journal of Biogeography 37:936–950. https://doi.org/10.1111/j.1365-2699.2009.02268.x

Martínez-Cabrera HI, Jones CS, Espino S, Schenk HJ (2009) Wood anatomy and wood density in shrubs: Responses to varying aridity along transcontinental transects. American Journal of Botany 96:1388–1398. https://doi.org/10.3732/ajb.0800237

Miles PD, Smith B (2009) Specific gravity and other properties of wood and bark for 156 tree species found in North America. US Department of Agriculture, Forest Service, Northern Research Station. https://doi.org/https://doi.org/10.2737/NRS-RN-38

Mitchard ET, Saatchi SS, Baccini A, et al (2013) Uncertainty in the spatial distribution of tropical forest biomass: a comparison of pan-tropical maps. Carbon Balance Manage 8:10. https://doi.org/10.1186/1750-0680-8-10

Morrison B (2018) Potential past and future tree migration responses to climate change. University of Illinois at Urbana-Champaign

Muller-Landau HC (2004) Interspecific and Inter-site Variation in Wood Specific Gravity of Tropical Trees. Biotropica 36:20–32. https://doi.org/10.1111/j.1744-7429.2004.tb00292.x

Nardini A, Battistuzzo M, Savi T (2013) Shoot desiccation and hydraulic failure in temperate woody angiosperms during an extreme summer drought. New Phytol 200:322–329. https://doi.org/10.1111/nph.12288

Phillips OL, Sullivan MJP, Baker TR, et al (2019) Species Matter: Wood Density Influences Tropical Forest Biomass at Multiple Scales. Surv Geophys 40:913–935. https://doi.org/10.1007/s10712-019-09540-0

R Core Team (2021). R: A language and environment for statistical computing. R Foundation for Statistical Computing, Vienna, Austria. URL https://www.R-project.org/.

Riegl Laser Measurement Systems GmbH. (2020). Riscan pro 2.0.

Rowe N, Speck T (2005) Plant growth forms: an ecological and evolutionary perspective. New Phytologist 166:61–72. https://doi.org/10.1111/j.1469-8137.2004.01309.x

Saldarriaga JG, West DC, Tharp ML, Uhl C (1988) Long-Term Chronosequence of Forest Succession in the Upper Rio Negro of Colombia and Venezuela. The Journal of Ecology 76:938. https://doi.org/10.2307/2260625

Santoro M, Cartus O, Carvalhais N, et al (2021) The global forest above-ground biomass pool for 2010 estimated from high-resolution satellite observations. Earth System Science Data 13:3927–3950. https://doi.org/https://doi.org/10.5194/essd-13-3927-2021

Stephenson N (1998) Actual evapotranspiration and deficit: biologically meaningful correlates of vegetation distribution across spatial scales. J Biogeography 25:855–870. https://doi.org/10.1046/j.1365-2699.1998.00233.x

Stephenson NL (1990) Climatic Control of Vegetation Distribution: The Role of the Water Balance. The American Naturalist 135:649–670. https://doi.org/10.1086/285067

Swaine MD, Whitmore TC (1988) On the definition of ecological species groups in tropical rain forests. Vegetatio 75:81–86. https://doi.org/10.1007/BF00044629

Swann ALS, Laguë MM, Garcia ES, et al (2018) Continental-scale consequences of tree die-offs in North America: identifying where forest loss matters most. Environ Res Lett 13:055014. https://doi.org/10.1088/1748-9326/aaba0f

Swenson NG, Enquist BJ (2007) Ecological and evolutionary determinants of a key plant functional trait: wood density and its community-wide variation across latitude and elevation. American Journal of Botany 94:451–459. https://doi.org/10.3732/ajb.94.3.451

ter Steege H, Hammond DS (2001) Character convergence, diversity, and disturbance in the tropical rain forest in Guyana. Ecology 82:3197–3212. https://doi.org/10.1890/0012-9658(2001)082[3197:CCDADI]2.0.CO;2

Van Gunst KJ, Weisberg PJ, Yang J, Fan Y (2016) Do denser forests have greater risk of tree mortality: A remote sensing analysis of density-dependent forest mortality. Forest Ecology and Management 359:19–32. https://doi.org/10.1016/j.foreco.2015.09.032

Wiemann MC, Williamson GB (1989) Wood Specific Gravity Gradients in Tropical Dry and Montane Rain Forest Trees. American Journal of Botany 76:924–928. https://doi.org/https://doi.org/10.2307/2444548

Wiemann MC, Williamson GB (2002) Geographic variation in wood specific gravity: effects of latitude, temperature, and precipitation. Wood and Fiber Science 34:96–107

Wiemann MC, Williamson GB (1987) Extreme radial changes in wood speicic gravity in some tropical pioneers. Wood and Fiber Science 20:344–349

Wikberg J, Ogren E (2004) Interrelationships between water use and growth traits in biomass-producing willows. Trees - Structure and Function 18:70–76. https://doi.org/10.1007/s00468-003-0282-y

Williamson GB, Wiemann MC (2010) Measuring wood specific gravity…Correctly. American Journal of Botany 97:519–524. https://doi.org/10.3732/ajb.0900243

Wickham H (2016). *ggplot2: Elegant Graphics for Data Analysis*. Springer-Verlag New York. ISBN 978-3-319-24277-4, https://ggplot2.tidyverse.org

Chapter 2. Deriving novel allometric equations for northern Sierra Nevada trees using terrestrial laser scanning

1. Introduction

Globally, the terrestrial biosphere, and in particular, forests, are estimated to provide a net sink of approximately 20% of carbon dioxide emitted by anthropogenic sources (Le Quere et al. 2017, Pan et al. 2011). Preserving forests following disturbances is thought to be important for anthropogenic $C0_2$ emissions uptake (Pugh et al. 2019). Creating carbon maps of forests at scales ranging from individual trees, to forested stands, to forests across the world rely on biomass equations created using either remote sensing data or field data. Specifically, in California's forests, drought and wildfire threaten forests and the wildland-urban interface and emphasizes the need for accurate carbon maps in this period of climate change. Long-term carbon storage and forest health predictors are complicated to identify without accurate data related to tree biomass (Pugh et al. 2018). Managing forests to increase carbon storage can be a strategy to mitigate climate change (Zheng et al. 2013) and depends on the availability of data and tools to monitor the change in forest biomass and carbon stocks over time (Galik et al. 2009). Carbon maps for forests are typically derived from either 1) remotely sensed data or 2) the Forest Inventory Analysis (FIA) dataset which estimates biomass across the continental US by using biomass equations to convert tree variables into estimates of biomass, and thus of forest carbon (Chave et al. 2004). These data create national maps of carbon stocks; however, national estimates of carbon are limited by the number of uncertainties produced from the variability of biomass equations and the heterogeneity present in a forest stand (Goetz et al. 2009).

These biomass equations, also known as allometric equations, are useful for estimating carbon sequestration of woody vegetation via its relationship between easy-to-measure tree metrics such as species, diameter-at-breast-height (DBH), and/or height. Allometry follows a basic principle in which proportions between tree height and diameter and between biomass and diameter follow rules that apply to all trees; with the increase of tree size, so increases tree variables, such as biomass, height, or diameter (King, 1996, Archibald & Bond, 2003, Bohlman & O'Brien, 2006, Dietze et al. 2008). This power-law relationship is applied to predict a tree component (biomass) from another tree component (diameter and height) and is based on the mechanical and hydraulic constraints of plant growth (West et al. 1999). Allometric equations are traditionally calibrated using destructive sampling to measure biomass, which is extremely costly, time-intensive, removes trees from the forest, and often does not take into account the full range of tree size, species, topoclimatic variability, or local stand conditions (Picard et al. 2012, Anderson-Teixeira et al. 2015). There is a noticeable lack of destructive sampling across local regions, which leads to under-representing a range of tree species and tree size, and also leads to allometric equations which tend to be applied outside of the populations which were sampled (Jenkins et al. 2003). Uncertainties are reduced with large sample sizes, as small sample size allometric models systematically overestimate carbons stocks in North America (Duncanson et al. 2015).

Terrestrial laser scanning (TLS) can be a solution for reducing uncertainties in allometric models, especially through direct estimates of AGB, as it is a way to increase sample sizes and reduce biases (Disney et al., 2019). TLS data can be used to characterize forest structure at a tree level, and tree parameters can be directly measured from the TLS

point cloud without sampling bias. TLS functions as an effective non-destructive alternative to destructive sampling, TLS can be used to sample large and hard-to-find trees as easily as the small and common tree species. As large trees can make up a total of 50% of the total live tree AGB, and inclusion of large trees in allometric models are vital to reducing uncertainty (Ahmed et al., 2013). However, the mm-accurate TLS point clouds introduce their own set of limitations and trade-offs, including low point density in the upper canopies of forests and occlusion in dense, tall forests (Burt et al., 2018).

TLS-derived AGB is estimated by calculating tree volume using quantitative structure models (QSMs; Raumonen et al., 2013), which reconstruct tree metrics by fitting cylinders to the trunk and branches. The QSM method estimates individual tree AGB when multiplied by wood specific gravity; however, wood specific gravity introduces more uncertainties in allometric models (Chave et al., 2006, Swenson and Enquist, 2007, Mitchard et al., 2013). QSMs have been applied for AGB estimation in boreal and temperate forests (Roumenen et al., 2015) and tropical forests (Disney et al., 2018, de Tanago et al., 2017). Calders et al. (2015) found that TLS derived AGB estimates in Australia had a high agreement with destructive sampling reference AGB (CV RMSE= 16.1%) compared to allometric model derived AGB (CV RMSE = 46.2% - 57%). Large tropical tree TLS-QSM derived AGB found a slightly higher agreement (CV RMSE = 28.37%), outperforming the accuracy of pantropical allometric models, providing evidence supporting a trend that TLS-derived volume c account for tree structure more effectively than allometric models and results in AGB estimates that are unbiased by tree size (de Tanago et al. 2017). Burt et al. (2013) found that volume derived from TLS data can be recreated to a 10.8% underestimate, and Wilkes et al.

(2018) found QSM recreated AGB to 1.4% overestimate for a local urban allometric equation in a London borough. TLS estimates of tree height have been found to be accurate compared to destructively sampled trees (Calders et al. 2015, Stovall et al. 2018), and since standard allometric models underrepresent large trees, TLS provides a unique opportunity to unbiasedly sample large trees.

Here, we developed novel TLS-derived allometric models across 16 tree species in the northern Sierra Nevada. California's northern Sierra Nevada forests have experienced an increase in drought and wildfire which threatens forests, and land managers are encouraged to manage forests to maintain forest health and ecosystem productivity (California Global Warming Solutions Act of 2006; Assembly Bill 32 (AB 32); Núñez, Chapter 488, Statutes of 2006). In order to create novel equations, we aim to improve upon the destructive harvesting approach and we will address the following limitations of that approach; i) small sample sizes ii) lack of full range of tree size sampled and iii) lack of diverse range of tree species and iv) region-specific equations that capture topoclimatic variability. We compared TLS-derived allometric models against existing national equations and evaluated the variability of TLS-derived allometric equations across a topoclimatic region using two water balance variables; climatic water deficit and annual actual evapotranspiration. We also assessed the use of QSMs for measuring tree structure metrics such as DBH and height. The effectiveness of TLS in estimating species-specific AGB to create novel allometric models may have large implications for future AGB and carbon stock estimations for the northern Sierra Nevada in a time of drastic change in forest biomass stocks.

2. Methods

2.1 Area of Interest (AOI) and plot selection

Our goal was to generate novel allometric equations for tree species in the Northern Sierra Nevada Mountains in California. As such, our primary areas of interest (AOIs) included the Lake Tahoe Basin Management Unit (LTBMU) and Plumas National Forest (PNF). These sites cover a large topoclimatic gradient spanning in elevation from 215 to over 2818 meters above sea level and cover approximately 5,200km^2. The northern Sierra Nevada Mountains experience a Mediterranean climate pattern of long, dry summers and cool, wet winters. Our dataset encompasses a large topoclimatic gradient and ranges in temperature from -9 ℃ to 28 ℃, in actual evapotranspiration (AET) from 348 to 476 (mm), and annual climatic water deficit (DEF) from 70 to 188 (mm) (Morrison, 2018).

Plot locations in the LTBMU and PNF were selected via a two-stage sampling design in which a grid of 10 km^2 was established covering the LTBMU and PNF, and 1 plot within each grid cell was randomly sampled, constrained to locations with > 10% tree cover taken from a LANDSAT analysis, and avoiding locations on private land, with heavy disturbances, such as recent fire history and logging based on CALVEG: A classification of California Vegetation mapping methodology (USDA Forest Service, 1981). In the end, we selected 108 plots located in California (Figure 1).

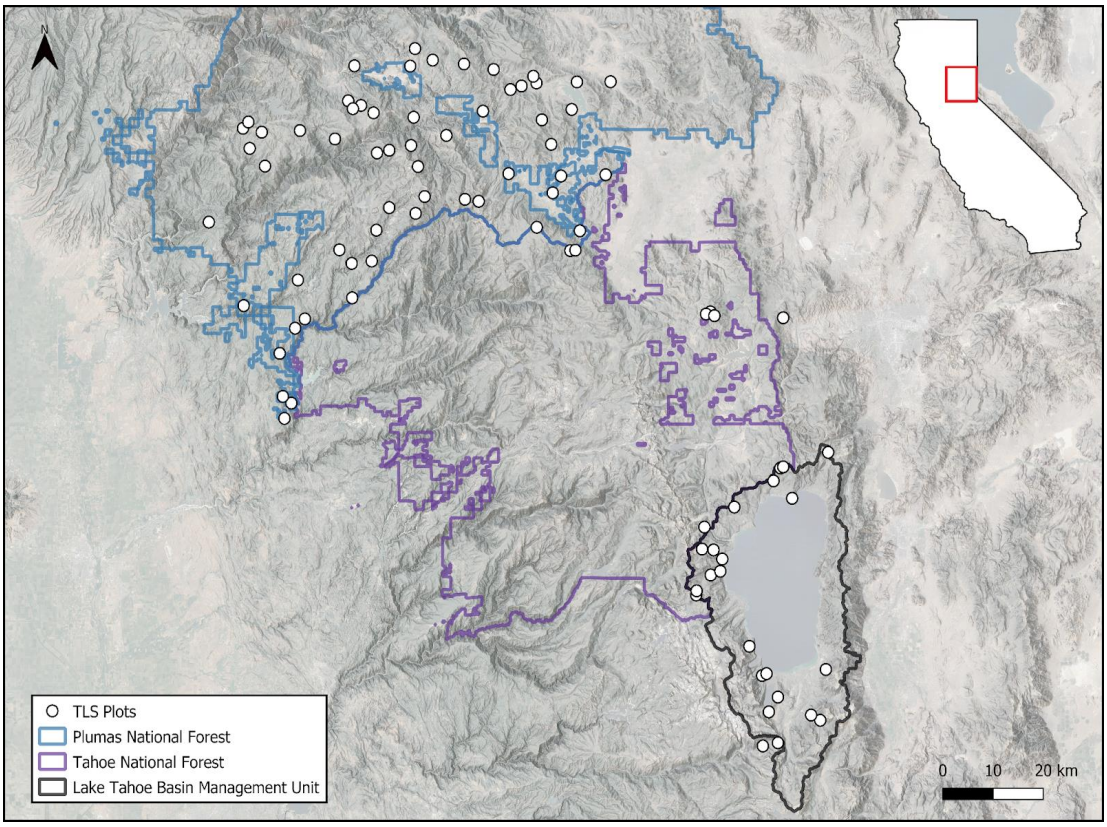

Figure 1. TLS plots (N=108) across the Plumas National Forest and Lake Tahoe Basin Management Unit (LTBMU). Three additional plots were placed outside of the Plumas NF and LTBMU boundaries to sample species that are not typically found in the Plumas NF and LTBMU, but occur outside of these areas in the northern Sierra Nevada.

2.2 Plot setup, initial field mensuration, and terrestrial laser scanning

Our plots were designed to represent a 30m x 30m area, with a 5m buffer on all sides. TLS data were acquired using a Riegl VZ-400i Terrestrial Laser Scanner, with specifications shown in Table 1. This instrument records multiple-return LiDAR data and collects data about the position and orientation of points in three-dimensional points. The TLS was mounted on a tripod, leveled at each scanning position, and the height of the tripod was adjusted at each to be higher than any surrounding shrubs or undergrowth to avoid occlusion. Each plot was scanned at 9-13 separate scanning positions (depending on the tree density of the plot) with terrestrial LiDAR during 3 field seasons from 2017 to

2019. Each scan was taken at an upright (0°) position and at a 30° tilt scan (to capture the tree canopies) at each scanning location. Additional scans were added to each plot depending on line-of-site from the TLS to each of the four reflectors located at four corners interior to the plot to establish a stable point across space and time and act as tie-points to co-register scan positions. Point clouds from each scan position were co-registered together using RiSCAN Pro software (Riegl Laser Measurement Systems GmbH, 2020). After coregistration, each TLS scan was registered to an airborne laser scanning (ALS) base map using LAStools (RapidLasso GmbH, 2019) and CloudCompare (Girardeau-Montaut, 2020), with an average point density of 7.86 points per cm^2 and 125,830,459 average number of points per plot and produced a detailed point cloud for each plot (Figure 2, Hartsook, 2021).

During the initial setup of plots in 2017, each plot was stem mapped in the field. An experienced forester identified the most dominant tree species in each plot, and any remaining tree species with a diameter ≥ 15 cm were identified and considered for stem mapping. The distance and azimuth to each tree within the plot were recorded from the plot center, which resulted in a complete stem map of tree species in each TLS plot (Hartsook, 2021).

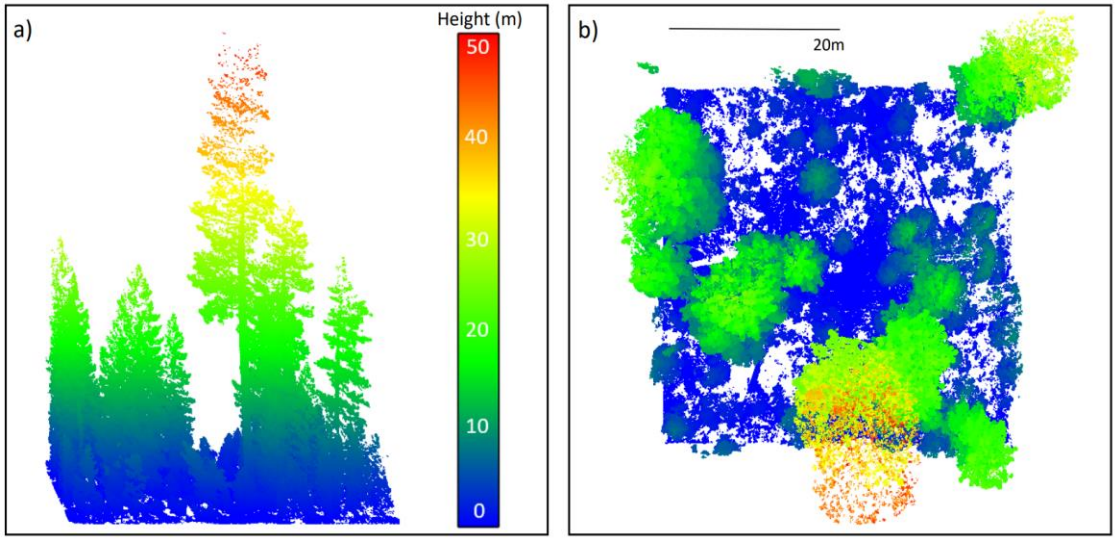

Figure 2. A TLS plot colored with a height ramp in meters **a)** as seen from a side view **b)** from a top-down view. Plots were clipped at 30 by 30 meters with a 5m buffer, and any noise associated with clipping the point cloud was taken care of by the 5 m buffer. As seen in **a)**, the TLS point density decreases with height, as the upper canopies of tall trees are harder to reach with the TLS.

TLS RIEGL VZ400i	Specifications
Wavelength	1550 nm
Minimum range	1.5 m
Maximum range	350 m
Scan range	0-360 ° in azimuth
	30-130 ° in zenith
Beam divergence	0.35 mrad
Scans per position	1 scan at 30 ° tilt
	1 scan at 0 ° tilt

Table 1. Riegl VZ-400i scanner settings for TLS multiple return data acquisition.

2.3 Ancillary data

Wood specific gravity sampling was outlined in Chapter 1. A total of 329 trees across 89 plots were cored for wood-specific gravity at DBH with a 5.15mm wide

increment borer. We removed pith and bark for each core prior to oven drying. For each tree core, we measured the basic wood specific gravity (WSG_b) as the ratio of oven-dried mass to green volume (WSG_b =oven dry mass/ green volume / ρ water) (Williamson and Wiemann, 2010). We obtained individual estimates of wood-specific gravity and calculated a species mean to multiply against TLS-derived volume to get AGB (equation 1). Each core sample was oven-dried for 48 to 72 hours in a well-ventilated oven at 101-105°C until the mass remained constant (Williamson and Wiemann, 2010). Green volume was measured using the water displacement method (Ilic et al. 2000), and the green volume of the sample is equal to the measured mass of the displaced water. A beaker was filled with deionized water and each sample was forced underwater using a small pin, with careful attention paid to each sample not touching the walls of the beaker. We obtained individual estimates of wood-specific gravity and calculated a species mean to multiply against TLS-derived volume to get AGB.

2.4 Tree selection

Our goal was to select trees for analysis that covered the diversity of species, size classes, and climatic conditions present across our study area. To accomplish this, we first created a stem map using virtual mensuration techniques, linking these stems against field-identified species. Each TLS point cloud was normalized to the height above ground using LAStools (RapidLasso GmbH, 2019), filtering all points within 5 cm of the standard DBH height 1.37m (1.32-1.42m). These DBH "slices" were converted to rasters at 1cm resolution (Figure 3). Each raster represented a TLS plot and trained researchers mapped diameter and tree species to each circle, which allowed for stem positions and DBH to be determined. Finally, these virtual stems were linked against all plot level

climate variables. This resulted in a polygon layer of tree positions, DBH, species, and climate variables for N = 5,873 trees (Hartsook, 2021).

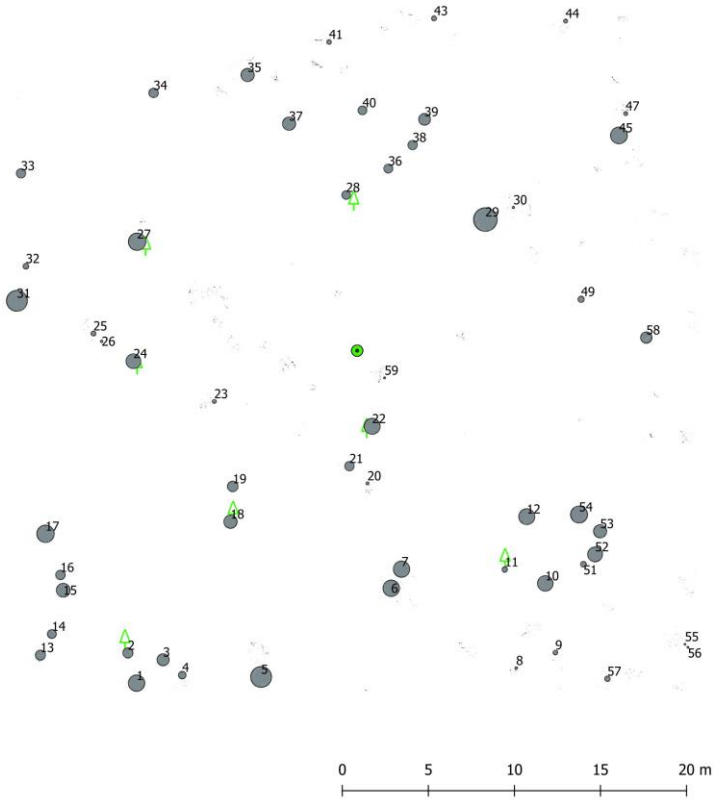

Figure 3. Virtual stem map of a TLS plot with tree ID, species and diameter assigned to each circle, which represents an individual tree in our plot. This results in a virtual stem map with trees represented as gray circles and each tree ID number assigned to each circle. The green tree icon next to each circle represents the field stem mapped trees that are not the dominant tree species assigned to each plot. Plot center is depicted by a green circle at the center of the stem map.

From this virtual stem map, we randomly selected trees stratified across species (16 tree species), size (in 10cm DBH bins, range 5cm to 178cm), and climate (in 25mm DEF bins, from 70 to 188mm). In total, 922 target trees were randomly selected across 16 tree species, 12 size classes (Figure 4a), and 6 climatic water deficit bins (Figure 4b). We revisited these trees in the field in 2020 and 2021 to re-confirm species and measured the DBH following standard field mensuration techniques.

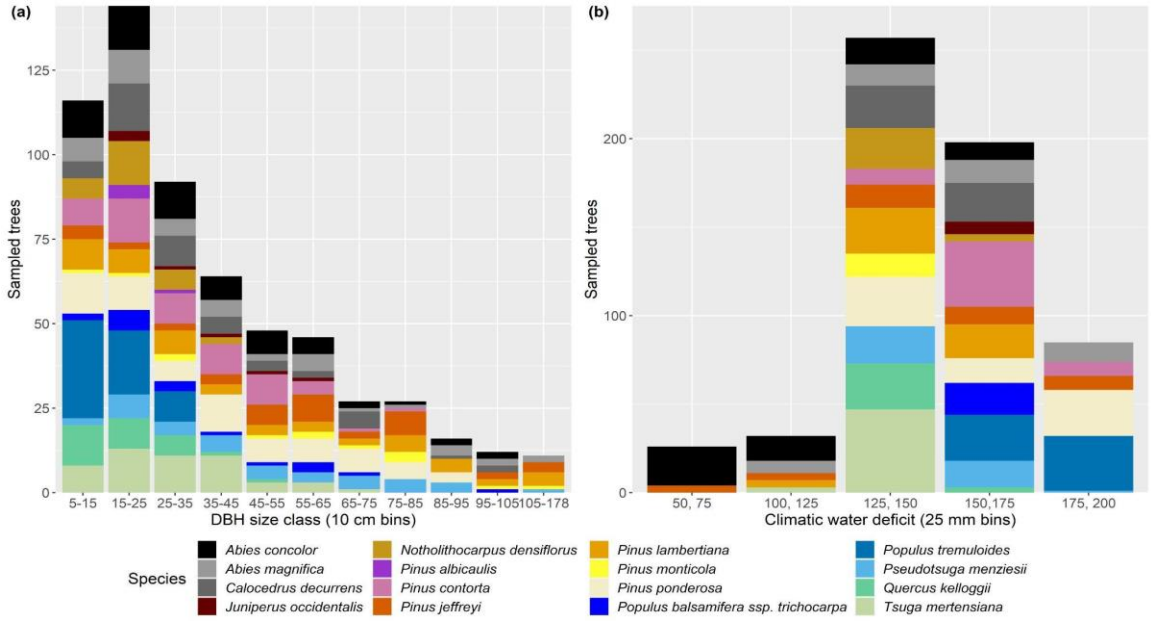

Figure 4. Target trees (n=922) were sampled at **a)** diameter size classes in 10 cm bins and **b)** climatic water deficit in 25 mm bins across 16 tree species in the northern Sierra Nevada.

2.5 Tree Biomass Estimation

Aboveground tree biomass (AGB_t, kg) for each tree of id *t* and species *s* in the previous step was estimated as the product of the tree's woody volume (V_t, m^3) and its wood specific gravity ($WSG_{s(t)}$, kg/m^3).

$$AGB_t = WSG_{s(t)} * V_t$$

Equation 1. Equation for estimation above ground biomass using TLS data

We used species' means of the wood specific gravity estimated in Chapter 1. The volume of each tree V_t was estimated from the TLS point cloud using TreeQSM (Raumonen et al. 2013). To estimate V_t, we first segmented the selected individual trees from the plot point cloud, removed points identified as leaves, and then processed the resulting leaf-off point cloud using TreeQSM.

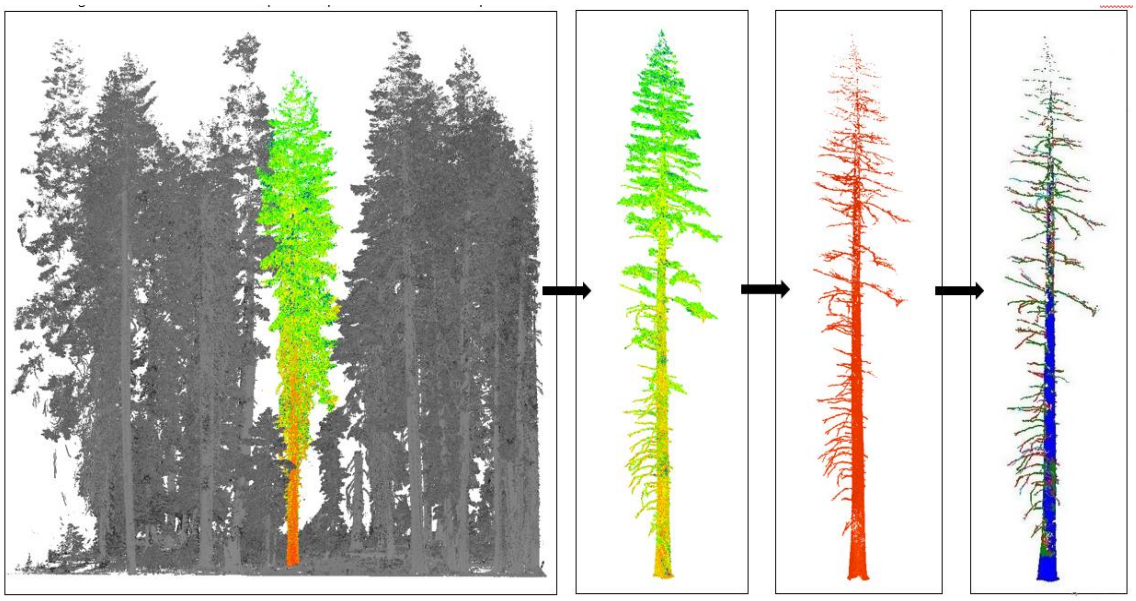

Figure 5. Individual tree segmentation from the 40x40m point cloud. Each tree ID was buffered with a 5 (trees ≤ 0.4m at DBH) or 10 m (trees ≥ 0.4m at DBH) buffer and exported as a text file before segmenting in Cloud Compare. All other vegetation, noise, and ground points were removed before filtering out the needles or leaves with the reflectance values in Cloud Compare. After that, the target tree was run in TreeQSM to obtain the volume and other tree metrics.

2.5.1 Tree Segmentation

For each tree selected in section 2.4, we did a coarse extraction of the tree's point cloud by clipping a cylindrical volume centered on the stem position with a radius of 5m if the DBH was less than 0.4m, and a radius of 10m if the DBH was greater than 0.4m. This cylindrical subset of the point cloud contained the entire target tree but also included ground and adjacent vegetation which needed to be removed before proceeding. Using Cloud Compare (Girardeau-Montaut, 2020), we manually removed all points belonging to the ground, adjacent plants, and other points deemed to not be part of the target trees. This process is diagrammed in Figure 5 and described in detail in the following sections.

2.5.2 Leaf removal

We removed points belonging to leaves from the target trees' point clouds by filtering the points' intensity values following the approach used by Hackenberg et al. (2015). The wavelength of the TLS (1550nm) is in one of the water absorption bands (Clevers and Schaepman, 2010), so lower intensities were more likely to be healthy, wet leaves as opposed to woody biomass. Kukko et al (2008) found that the increasing incidence angle led to decreasing intensity values. It follows that leaves and needles are irregular and planar surfaces that increase the intensity angle of the laser beam (Pesci and Teza, 2008). The specific intensity thresholds were set individually for every tree in our dataset using visual inspection to determine that only the leaves were removed and not the trunk or branches. Wilkes et al. (2018) found the tree crown small diameter branches ($\leq$ 20cm) represent a high proportion of tree volume in urban trees in London boroughs, so our goal for this protocol was to keep as many small branches as possible while still retaining high point density. Although we lost some small branches at the top of the tree due to setting an intensity threshold, the integrity of the branching structure in the canopy remained for the majority of the trees. We erred on the side of leaving some needles while keeping the point density for the top of the trees as high as possible.

2.5.3 Quantitative Structure Models

We used TreeQSM to directly estimate tree volume from the resultant individual leaf-off tree point clouds (Raumonen et al. (2013). TreeQSM estimates volume by using patches on the surface of the tree to fit cylinders that reconstruct the volume and structure of the trunk and branches. The patch sizes of each pass with TreeQSM are an important parameter to be modified depending on the size and occlusion level of the tree. Some

main assumptions of the QSM reconstruction method are (i) the input point cloud is a single tree (ii) the tree has to have sufficiently high point density to be reconstructed (iii) leaves and needles need to be removed or the tree needs to be scanned during a leaf off conditions (iv) the tree architecture can be reconstructed with cylinders (v) branches taper and the child branch is always smaller than the parent branch and (vi) there are no assumptions about tree species or size.

Before reconstructing our target trees with TreeQSM, we down sampled each individual tree point cloud to 1 point per cm3 using the *cubical_down_sampling* function. For each tree, we began by setting the TreeQSM input parameters PatchDiam1, PatchDiam2Max, PatchDiam2Min, BallRad1 and BallRad2 to the default recommendations suggested by the TreeQSM documentation (Raumonen et al. 2020), which also suggests optimizing input parameters according to height and occlusion level. From this starting point, we adjusted input parameters based on three height classes of trees with high point density and not too much occlusion: 2-10 m, 10-30m, and 30-50m. For trees with lower point density and high levels of occlusion, we increased the input parameters so that the patch cover sizes would be larger. We initially ran 5 models using these input parameters using the *make_models* function and selected the optimal models using the *select_optimal* function. We finalized the model by running the *make_models* function again to produce 20 models. Finally, we ran the *estimate_precision* function which results in the best estimate of the mean, standard deviation, and the coefficient of variation (%) for all tree metrics. We analyzed the final estimates by 1) visual inspection and 2) standard deviation and coefficient of variation (%). We removed trees by visual inspection in which branches were askew, did not connect, and/or were floating in midair,

or did not follow the branching structure of the original tree's point cloud as seen in Cloud Compare. We also removed trees that had a high mean volume standard deviation and a coefficient of variation of mean volume ≥ 15 %. We retained the estimated tree volume, tree height, and tree diameter for subsequent analysis. We used Matlab (The MathWorks Inc. 2019) for all QSM reconstructions.

2.5.4 Aboveground biomass estimation and final database

For each tree, we estimated the tree's aboveground biomass following equation (1) using the TreeQSM estimated volume and the mean wood specific gravity for that tree's species. Our final database was:

TreeID,TreeXY,Species,DEF,DBH_{field},DBH_{QSM},$Height_{QSM}$,AGB_{QSM}

2.5.5 TreeQSM accuracy assessment

While we did not have independent data to validate the volume measurements, we did have field measurements of DBH in cm (N=386) and height in m (N=197) to compare against the TreeQSM estimates of these parameters.

2.6 Allometric Models

2.6.1 Allometric model development

Allometric equations were created to estimate species-specific biomass AGB_s. We investigated three (3) different equations using different sets of structural predictor variables (DBH and height), for use in different applications. Additionally, we investigated the utility of a climate-enhanced allometric model to see if climatic water deficit and actual evapotranspiration modified the relationships between AGB and their structural predictors. Table 2 describes the model forms and their applications.

Model predictors	Model Form	Utility
DBH	$AGB_s = \exp(\beta_0 + \beta_1 \ln(DBH))$	Common rapid collection equation
DBH and height	$AGB_s = \exp(\beta_0 + \beta_1 \ln(DBH^2 * Height))$	Common rapid collection equation
Height	$AGB_s = \exp(\beta_0 + \beta_1 \ln(Height))$	For use with airborne LiDAR datasets
AET and DEF	Mixed effect model	Topographic gradient analysis

Table 2: Allometric equation predictors, form and utility

We performed a stratified, largely random sampling based on species to select 75% of the trees from our database (N=454) to derive our models, reserving 25% of the data (N = 151) for an independent validation. The exception to the true randomness was, for each species, we included the smallest and largest tree by volume (L) in our calibration dataset. Using our calibration dataset, we used ordinary least squares log-linear regression as described in Picard et al. (2012) to determine the scaling coefficient, β_1, and intercept, β_o, for three forms (DBH-only, DBH, and height, height-only). Although log-linear regressions tend to underestimate the predicted metrics in circumstances of high RMSE unless a correction factor is applied to back transform the log units (Baskerville, 1972, Sprugle, 1983, Clifford et al. 2013), we decided the correction factor might bias models with small sample sizes (Flewelling and Pienaar,

1981). Using the validation dataset, we evaluated the models using the concordance correlation coefficient (CCC), RMSE in kg, relative RMSE (%, calculated using 10cm DBH bins), and % bias. The climate-enhanced model approach is described below.

2.6.2 Allometric model analysis

Model uncertainty was calculated as CCC, RMSE, relative RMSE, Bias (kg), and % Bias.

$$\text{Relative RMSE (\%)} = \text{RMSE}_{\text{10 cm DBH bin)}} / \text{mean AGB}_{\text{10 cm DBH bin}} * 100$$

Equation 2. Relative RMSE equation

Where y_i is the AGB values predicted by the allometric models and y is the TLS-QSM AGB estimates in kg. The relative RMSE (%) was calculated for each DBH 10-cm bin and divided by the mean AGB of each 10 cm bin, since RMSE increases with larger diameters and is highly dependent on sample size (Equation 2) as described in Stovall et al. (2018). We then averaged all the relative RMSE values at each DBH size class for the general all species allometric models and species-specific models. Relative RMSE (%) provided a more representative RMSE for each species. All analyses were conducted in R version 4.1 (R Core Team, 2021).

2.6.4 Comparison to national equations

Our allometric equations were compared to commonly used national equations for the United States (Jenkins et al. 2003, Chojnacky et al. 2014). We calculated CCC, RMSE, relative RMSE, and bias for each model. We compared the national biomass estimates from Jenkins et al. (2003) and Chojnacky et al. (2014) to the TLS-QSM biomass using RMSE and bias, although Chojnacky et al. (2014) does not report RMSE values and only reports bias.

2.6.5 The effect of climate on AGB

We evaluated AGB variation across species over the northern Sierra Nevada topoclimatic region. We included diameter, height, species, and plot-level climate information (e.g. temperature, elevation, precipitation, climatic water deficit, and actual evapotranspiration) as potential predictor variables in a linear mixed-effects model with Plot ID as a random effect (Table 3). To determine if climate, in particular, influenced AGB variation, we focused on two water balance parameters, annual climatic water deficit (mm) (DEF) and annual actual evapotranspiration(mm) (AET) derived for each plot (Morrison, 2018). Methods for deriving these climate variables for each of our TLS plots located in California are included in Morrison (2018). Climate variables were downscaled from a continuous geospatial database using statistical downscaling techniques that incorporates topographic and spatial features at a finer scale. Coarse scale general circulation model climate grids were collected into a 30-year average and calibrated with weather station data. While statistically downscaling can allow for fine scale spatial features, the performance of downscaled variables can vary; for example, downscaled results performed worse for annual minima compared to annual maxima (Fowler et al. 2007).

Scientific Name	Common name	Sample size (n)	Elevation (m)	Temperature Range (°C)	Annual Precipitation (mm)	Annual Climatic Water Deficit (mm)	Annual Actual Evaportanspiration (mm)
Abies concolor	White Fir	60	1443-2334	-8 to 26	2786-3353	124-175	363-445
Abies magnifica	Red Fir	45	1611-8364	-8 to 25	2372-3353	109-176	348-422
Calocedrus decurrens	Incense Cedar	46	890-2019	-5 to 27	2932-3812	133-170	390-454
Juniperus occidentalis	Western Juniper	14	1443-2627	-5 to 26	3309	168	445
Notholithocarpus densiflorus	Tan Oak	25	890-944	-2 to 27	3826-3921	13-147	451-471
Pinus albicaulis	Whitebark Pine	6	2817	-7 to 24			
Pinus contorta	Lodgepole Pine	54	1782-2334	-7 to 25	2372-2993	139-177	352-414
Pinus jeffreyi	Jeffrey Pine	26	856-2222	-7 to 25	2766-3668	124-177	362-445
Pinus lambertiana	Sugar Pine	49	1228-2002	-7 to 26	2766-3674	124-147	390-463
Pinus monticola	Western-white Pine	14	1865-2208	-7 to 27	2799-2928	125-156	375-404
Pinus ponderosa	Ponderosa Pine	67	890-1780	-7 to 27	2814-3668	124-188	395-438
Populus balsamifera ssp. trichocarpa	Black Cottonwood	19	1472-1917	-5 to 25	2933-3117	140- 159	408-437
Populus tremuloides	Quaking Aspen	57	1817-1917	-7 to 25	2593-2896	166-177	392-417
Pseudotsuga menziesii	Douglas Fir	40	535-1542	-5 to 27	3338-3916	143-177	268-272
Quercus kelloggii	Black Oak	30	760-1618	-4 to 27	3338-4051	124-177	425-461
Tsuga mertensiana	Mountain Hemlock	50	718-2549	-9 to 23	2512-2748	109-139	377-381

Table 3. For each species, we included the ranges for elevation (m), temperature (°C), annual climatic water deficit (DEF) (mm), and annual actual evapotranspiration (AET) (mm). The blank spaces indicate no climate information for plots located in Nevada that were opportunistically sampled for *Pinus albicaulis* that was not found in our California dataset and for which we did not have climate information.

We evaluated the Pearson correlation coefficient between AET and DEF and determined that the variables were uncorrelated ($r < 0.65$) with variance inflation factors less than 5 from the car package (Weisberg, 2019) to check for multicollinearity. We used F-test Anovas to determine if the predictor variables explained the variance in AGB. We used non-linear mixed-effects models with the lmer function in the lme4 package (Bates et al. 2015) in R version 4.1.1 (R Core Team, 2021), but determined that the residuals of the linear mixed-effects model were not normal. Instead, we ran a log-transformed mixed-effects model which had normally distributed residuals. We used unscaled variables to ensure ease of interpretation of the results. Plot was included as a random effect because we are trying to make an inference about the entire topoclimatic

region of the northern Sierra Nevada, and this way we can try to account for the random effect that plot locations contribute.

We reported the outputs of the linear mixed-effects model as the parameter estimates (β), p-values, and Pseudo-R^2 values (Table 7) along with the effect sizes of each predictor variable (Figure 12).

3. Results

3.1 TreeQSM measurement validation

Compared to field measurements, we found that TreeQSM yielded a correlation for DBH of 0.98 and a RMSE of 4.7cm. For height, TreeQSM yielded a correlation of 0.97 and a RMSE of 2.24m. Figure 6 shows the scatter plot of field vs. TreeQSM estimates of these metrics.

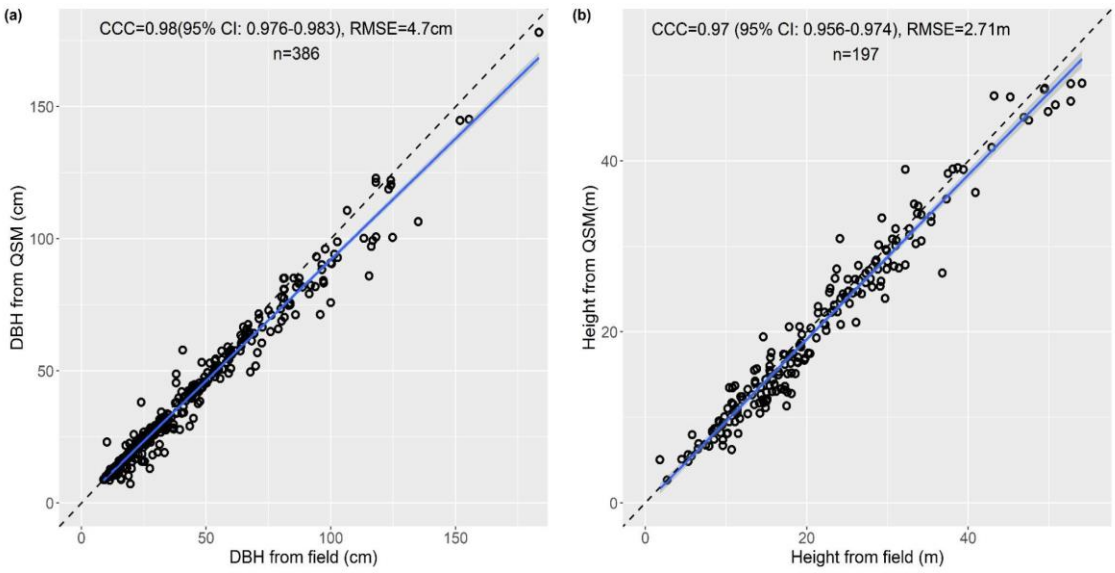

Figure 6. The comparison of field-measured (a) DBH and (b) height against TreeQSM-derived DBH and height. The dotted black line depicts a 1:1 line, the blue line shows the linear fit, and the gray bars display the 95% confidence interval.

3.2 TLS Allometry

We created 606 QSM models to develop 48 species-specific allometric models across the northern Sierra Nevada. Per-species sample sizes ranged from 6 to 67. Trees ranged from 5 to 178 cm in DBH and 2 to 51 m in height. Volumes ranged from 19 to 56268 L and AGB ranged from 10 to 27852 kg.

We derived three structural-based allometric models for the validation data for all species combined: DBH-only, DBH and height, and height-only (Figure 7). Validation of these TLS allometric models was conducted with a 75% (454 trees) training dataset used to train the least square log-linear regression models which predict AGB and a 25% (151 trees) testing dataset of TLS-QSM AGB, where the testing dataset was the only data used for validation. We produced error indications relating to the error of the TLS-QSM AGB values predicted by the log-linear regression models. The DBH-only equation performed the best with an RMSE of 738kg, Bias of 53.9 kg, and CCC of 0.95. The addition of height to the DBH equation did not improve the model and led to an increase in RMSE to 807 kg and a decrease in CCC to 0.93. The height-only equation performed the worst out of all three equations and had an RMSE of 1337 kg and a CCC of 0.73.

In addition to general allometric models, we produced three allometric equations (DBH-only, DBH and height, and height-only) on the validation data for 16 tree species (Figure 7). The DBH-only allometric equations yielded CCCs ranging from 0.69 to 0.98, RMSEs ranging from 29kg to 3670 kg, and relative RMSE (%) ranging from 9 to 39% (Table 4, Figure 8). The DBH-Height equation yielded CCCs from 0.83 to 0.98, RMSEs from 34 to 3374 kg, and relative RMSE (%) from 9.3 to 39.5 (Table 5). The height-only allometric equation had the highest ranging CCCs from 0.23 to 0.95, RMSEs ranging

from 32 to 4724 kg, and relative RMSE from 12.3 to 64.2 (Table 6). Tables 4, 5, and 6 show the allometric equation coefficients and accuracy results for each species, as well as the general (all-species) model.

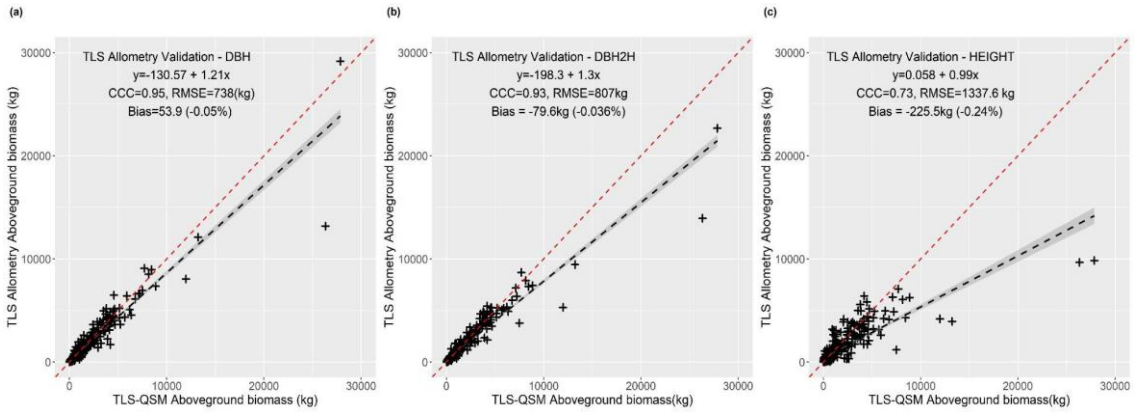

Figure 7. Linear regressions on the validation data comparing TLS-QSM AGB estimates against AGB predicted by the three different TLS allometric models for all species **a)** DBH **b)** DBH^2H **c)** Height. We used a testing dataset of 151 trees to predict AGB against the training dataset of 454 trees. We included the smallest and largest tree by volume in our testing dataset and made sure to stratify sampling evenly across all species so that species with a small sample size would be equally represented. The predicted AGB is underestimated compared to the observed AGB for all equations with a CCC of 0.95 for the DBH allometric equation, CCC=0.93 for the DBH^2H allometric equation, and a CCC of 0.73.

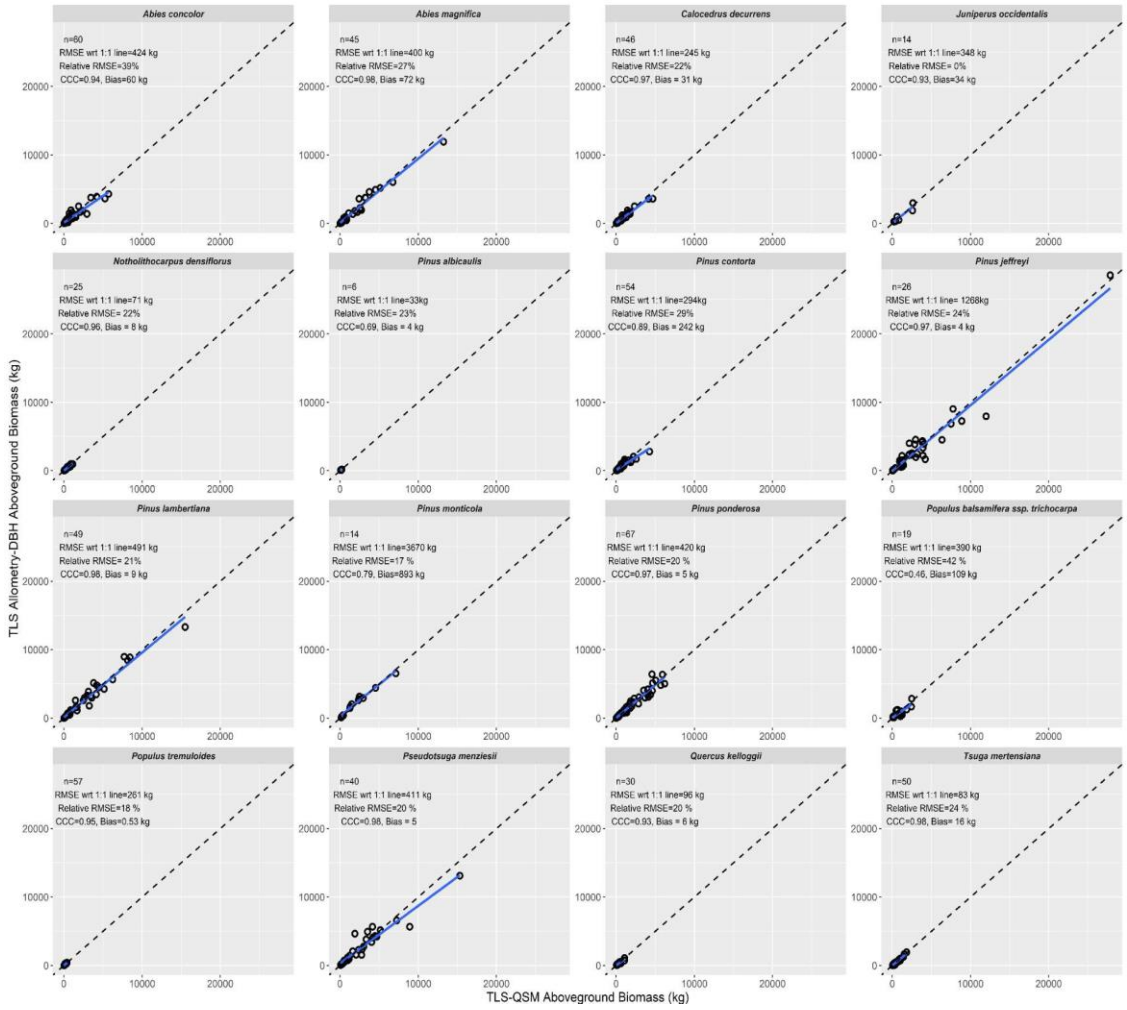

Figure 8. TLS Allometric-DBH models predicting biomass on the validation data across 16 tree species with sample size, RMSE, relative RMSE, CCC, and bias values are shown in the top left corner. The dotted line is a 1:1 relationship; the solid blue line depicts the linear fit.

General and Species-Specific Allometry													
Equation	**Species**	**n**	**DBH (cm)**	**ß0**	**ß0 [se]**	**ß1**	**ß1 [se]**	**CCC**	**RMSE (log units)**	**RMSE (%)**	**RMSE (kg)**	**Bias (kg)**	**% Bias**
DBH	*All Species*	606	15-175	-1.442	0.08	2.2	0.023	0.95	0.32	35	738	53.90	-0.05
	Abies concolor	60	11-100	-1.302	0.31	2.1	0.087	0.94	0.41	39	424	60.00	-0.10
	Abies magnifica	45	6-145	-1.545	0.21	2.2	0.057	0.98	0.26	27	400	71.90	-0.04
	Calocedrus decurrens	46	11-100	-1.815	0.27	2.2	0.077	0.97	0.33	22	245	31.00	-0.05
	Juniperus occidentalis	14	15-61	-0.860	1.24	2.1	0.355	0.93	0.32	0	348	34.00	-0.05
	Notholithocarpus densiflorus	25	7-038	-1.048	0.30	2.2	0.099	0.96	0.21	22	71	7.50	-0.02
	Pinus albicaulis	6	15-25	0.877	2.28	1.3	0.758	0.69	0.26	23	33	4.00	-0.36
	Pinus contorta	54	12-075	-1.616	0.30	2.2	0.086	0.89	0.31	29	242	14.00	-0.05
	Pinus jeffreyi	26	10-120	-2.281	0.35	2.4	0.089	0.97	0.36	24	1268	4.00	-0.07
	Pinus lambertiana	49	6-145	-1.992	0.17	2.3	0.045	0.98	0.24	21	491	9.40	-0.03
	Pinus monticola	14	11-175	0.019	0.44	1.8	0.107	0.79	0.28	17	3670	893.00	-0.04
	Pinus ponderosa	67	6-090	-2.085	0.14	2.4	0.038	0.97	0.22	20	420	4.60	-0.03
	Populus balsamifera ssp. trichocarpa	19	12-095	0.119	0.95	1.7	0.271	0.85	0.73	42	366	52.00	-0.30
	Populus tremuloides	57	6-031	-1.413	0.20	2.2	0.075	0.95	0.23	18	261	0.53	-0.30
	Pseudotsuga menziesii	40	12-132	-1.505	0.28	2.3	0.074	0.98	0.19	20	411	5.00	-0.02
	Quercus kelloggii	30	9-048	0.210	0.48	1.7	0.167	0.93	0.31	20	96	12.00	-0.05
	Tsuga mertensiana	50	6-070	-0.533	0.31	1.9	0.094	0.98	0.33	24	83	16.00	-0.05

Table 4. General and species-specific TLS derived allometric models*, their parameters, and the validation results. B_0 and B_1 are the regression coefficients and each coefficient's standard error is given. Error-values are displayed as the CCC, RMSE (kg), relative RMSE (%), MAE (kg) and Bias (kg).

*Biomass equation (2): $AGB = \exp(B_0 + B_1 \ln(DBH))$

General and Species-Specific Allometry													
Equation	Species	n	DBH (cm)	ß0	ß0 [se]	ß1	ß1 [se]	CCC	RMSE (log units)	RMSE (%)	RMSE (kg)	Bias (kg)	% Bias
DBH2H	*All Species*	606	15-175	-1.59	0.068	0.79	0.007	0.93	0.26	28.4	810	79.60	-0.040
	Abies concolor	60	11-100	-1.51	0.246	0.78	0.025	0.98	0.32	18.2	274	14.00	-0.070
	Abies magnifica	45	6-145	-1.34	0.153	0.76	0.015	0.95	0.19	19.4	669	113.00	-0.020
	Calocedrus decurrens	46	11-100	-1.74	0.154	0.78	0.016	0.97	0.19	13.8	247	35.00	-0.020
	Juniperus occidentalis	14	15-61	-1.41	0.903	0.88	0.099	0.96	0.23	9.3	269	18.00	-0.030
	Notholithocarpus densiflorus	25	7-038	-1.79	0.274	0.84	0.032	0.96	0.17	16.0	81	3.10	-0.010
	Pinus albicaulis	6	15-25	0.29	0.850	0.56	0.103	0.92	0.12	12.5	20	0.96	-0.007
	Pinus contorta	54	12-075	-1.75	0.236	0.79	0.024	0.94	0.21	21.8	180	10.70	-0.020
	Pinus jeffreyi	26	10-120	-1.75	0.339	0.83	0.031	0.95	0.40	28.6	1559	387.00	-0.080
	Pinus lambertiana	49	6-145	-1.90	0.013	0.81	0.013	0.97	0.21	16.4	448	29.30	-0.020
	Pinus monticola	14	11-175	-0.75	0.512	0.72	0.045	0.83	0.29	24.4	3374	800.30	-0.040
	Pinus ponderosa	67	6-090	-1.77	0.126	0.81	0.012	0.99	0.21	15.1	270	26.60	0.030
	Populus balsamifera ssp. trichocarpa	19	12-095	-1.40	0.900	0.75	0.090	0.86	0.57	39.5	355	52.00	-0.170
	Populus tremuloides	57	6-031	-1.99	0.210	0.83	0.027	0.93	0.21	20.1	34	2.50	-0.020
	Pseudotsuga menziesii	40	12-132	-1.87	0.240	0.83	0.022	0.98	0.14	17.7	372	51.00	-0.010
	Quercus kelloggii	30	9-048	-0.23	0.472	0.67	0.059	0.91	0.29	19.8	128	35.00	-0.150
	Tsuga mertensiana	50	6-070	-0.81	0.167	0.71	0.018	0.98	0.33	16.9	83	16.70	-1.200

Table 5. General and species-specific TLS derived allometric models*, their parameters, and the validation results. B_0 and B_1 are the regression coefficients and each coefficient's standard error is given. Error-values are displayed as the CCC, RMSE (kg), relative RMSE (%),and Bias (kg).

*Biomass equation (3): $AGB = \exp(B_0 + B_1 \ln(DBH^2 * Height))$

General and Species-Specific Allometry														
Equation	**Species**	**n**	**DBH (cm)**	**ß0**	**ß0 [se]**	**ß1**	**ß1 [se]**	**CCC**	**RMSE (log units)**	**RMSE (%)**	**RMSE (kg)**	**Bias (kg)**	**% Bias**
Height	*All Species*	606	15-175	-0.32	0.14	2.28	0.048	0.73	0.61	30	1485	225.0	-0.20
	Abies concolor	60	11-100	-0.32	0.47	2.12	0.174	0.91	0.69	23	508	125.0	-0.17
	Abies magnifica	45	6-145	-0.44	0.25	2.32	0.085	0.75	0.38	14	1493	286.0	-0.07
	Calocedrus decurrens	46	11-100	-0.21	0.36	2.22	0.133	0.69	0.53	22	725	127.5	-0.14
	Juniperus occidentalis	14		-1.33	1.07	3.61	0.487	0.95	0.27	52	279	87.0	-0.04
	Notholithocarpus densiflorus	25	7-038	-0.61	0.93	2.27	0.345	0.77	185.00	64	180	48.0	-0.23
	Pinus albicaulis	6	15-25	2.90	0.63	0.92	0.280	0.78	0.17	20	32	2.3	-0.02
	Pinus contorta	54	12-075	0.23	0.49	2.00	0.171	0.86	0.39	20	252	42.0	-0.08
	Pinus jeffreyi	26	10-120	0.88	0.58	2.15	0.193	0.48	0.86	30	4116	1097.4	-0.50
	Pinus lambertiana	49	6-145	-1.20	0.28	2.59	0.094	0.91	0.41	24	977	-127.3	-0.09
	Pinus monticola	14	11-175	-0.95	1.56	2.60	0.486	0.62	0.74	12	4724	1328.5	-0.27
	Pinus ponderosa	67	6-090	-0.31	0.31	2.26	0.101	0.89	0.60	24	721	196.8	-0.16
	Populus balsamifera ssp. trichocarpa	19	12-095	-0.78	1.49	2.21	0.481	0.23	0.61	29	689	215.0	-0.59
	Populus tremuloides	57	6-031	-1.30	0.54	2.42	0.227	0.59	0.48	29	74	14.0	-0.12
	Pseudotsuga menziesii	40	12-132	-1.84	0.49	2.74	0.149	0.87	0.40	32	949	242.9	-0.09
	Quercus kelloggii	30	9-048	1.70	0.76	1.48	0.320	0.55	0.62	20	205	59.8	-0.18
	Tsuga mertensiana	50	6-070	0.99	0.38	1.83	0.147	0.82	0.56	53	241	58.0	-0.28

Table 6. General and species-specific TLS derived allometric models*, their parameters, and the validation results. B_0 and B_1 are the regression coefficients and each coefficient's standard error is given. Error-values are displayed as the CCC, RMSE (kg), relative RMSE (%), and Bias (kg).

*Biomass equation (3): $AGB = \exp(B_0 + B_1 \ln(Height))$

3.3 National biomass equations comparison

When compared to TLS-QSM derived AGB, the national-scale equations overestimated biomass and had generally larger RMSE (log unit) values, especially with the inclusion of large trees. Each species agreed with national scale allometric models differently. For example, TLS-QSM AGB for *Notholilthocarpus densiflorus*, tan oak, demonstrated high agreement with both national models and TLS allometry. *Tsuga mertensia, Abies magnifica, Abies concolor,* and *Quercus kelloggii* exhibited lower TLS allometry and TLS-QSM derived AGB estimates compared to national scale models. Species with very large trees, *Pinus monticola and Pinus jeffreyii,* showed a very clear

distinction in how the extremely large trees' biomass is estimated when comparing TLS allometry to national equations. Figure 9 displays the species-specific comparison of national allometric models, TLS-derived allometric models, and TLS-QSM AGB.

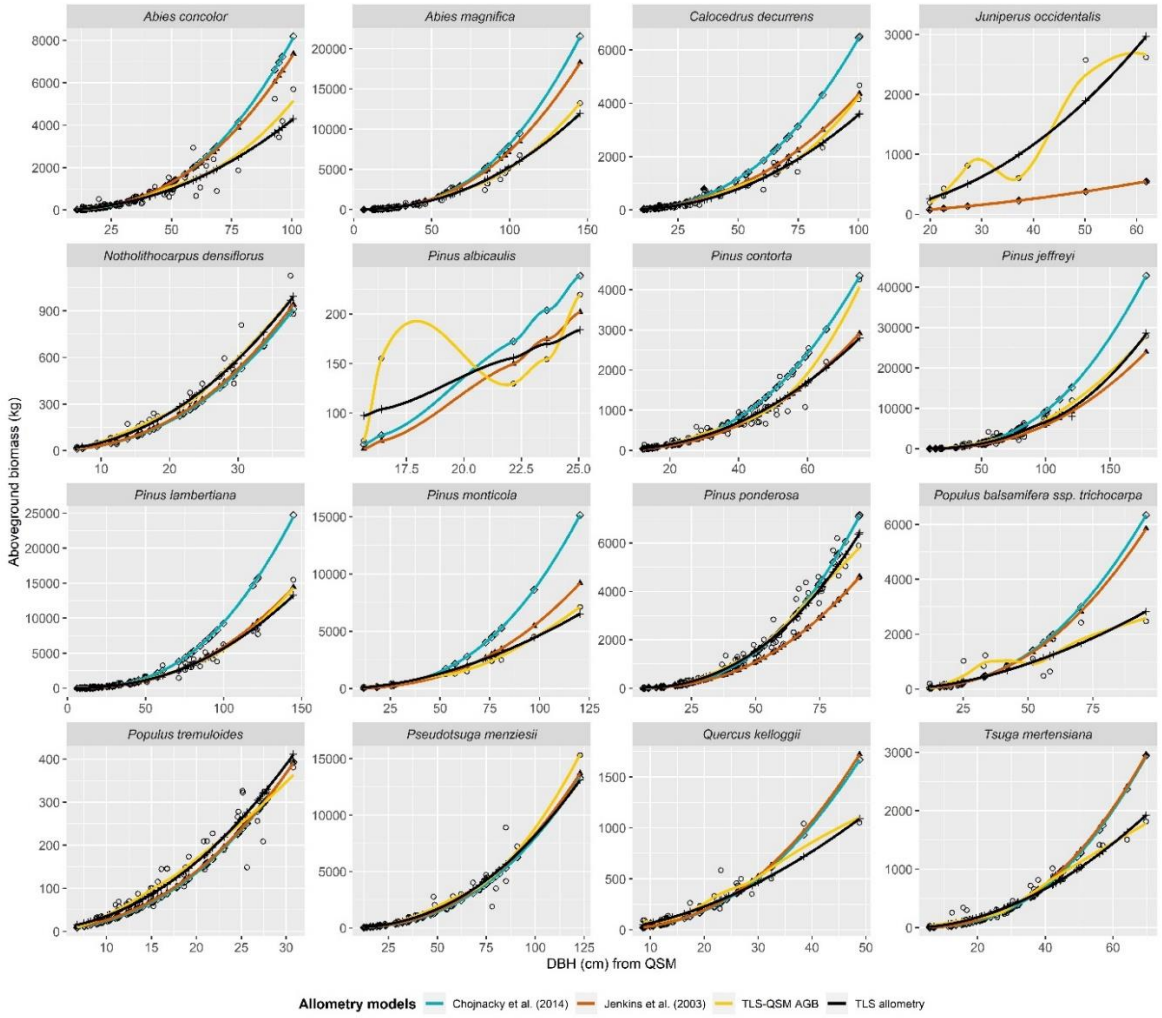

Figure 9. AGB estimates (kg) for each tree species with sample size and error values included in the upper left-hand corner: 1) the red line of Jenkins et al. (2003) AGB estimates, 2) the blue line of Chojnacky et al. (2014) AGB estimates national biomass equations, 3) the yellow line of TLS-QSM derived AGB estimates, and 4) TLS allometry AGB estimates shown in black. TLS allometry tends to have lower estimates of AGB across all tree species, and dramatically lower estimates of AGB in *Pinus monticola*. Certain tree species TLS allometry agreed more with the Jenkins et al. (2003) national equations (*Pinus jeffreyi, Pinus lambertiana, Tsuga mertensiana, Pseudotsuga menziesii,* and *Populus tremuloides*). Chojnacky et al. (2014) did not agree with TLS allometry or TLS-QSM AGB across most species and tended towards estimating higher AGB compared to other methods.

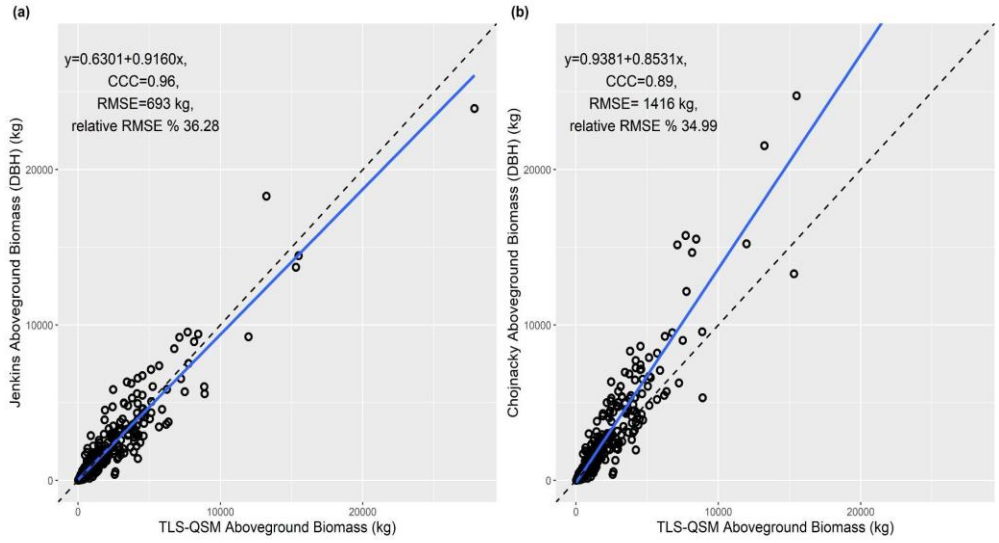

Figure 10. Examples of plots comparing different allometric models against TLS-QSM AGB in kilograms across all species in our dataset. All allometric models are using species-specific equations, and all estimated AGB values are plotted on the y axis against TLS derived AGB (kg) against **a)** Chojnacky et al. (2014) allometric predictions and **b)** Jenkins et al. (2003) allometric predictions.

3.4 Variability of AGB with climate

Our goal was to determine the climate effect and direction on AGB, with AET (mm) and DEF (mm) as our two main climate predictor variables. We ran F-test Anovas to see which predictor variables explained any variance in AGB. We found that DEF had a negligible effect (intercept = 2115.656, p-value=0.1763, and a R^2 = 0.003) and AET also did not have an effect on the strength or direction of AGB (intercept=1219.46, p-value=0.544, R^2=0.0006). We ran log-transformed mixed-effects models using AET, DEF, DBH, and Height as predictor variables with Plot as a random effect and evaluated that the residuals on the log-transformed model were relatively normal. The effect of AET and DEF on TLS-QSM derived AGB was not significant (Table 7); there were no trends of topoclimatic variability across a region on AGB and the climate variables had

no effect (Figure 12). After evaluating these results, we determined that climate had a negligible effect on allometric equation variability. However, if we look at individual species' AGB variability, we saw that *Pinus monticola*, *Pinus lambertiana*, and *Pseudotsuga menziesii* biomass decreased with increased climatic water deficit (Figure 11). This means that biomass for those tree species was lower in sites that were drier or under drought stress.

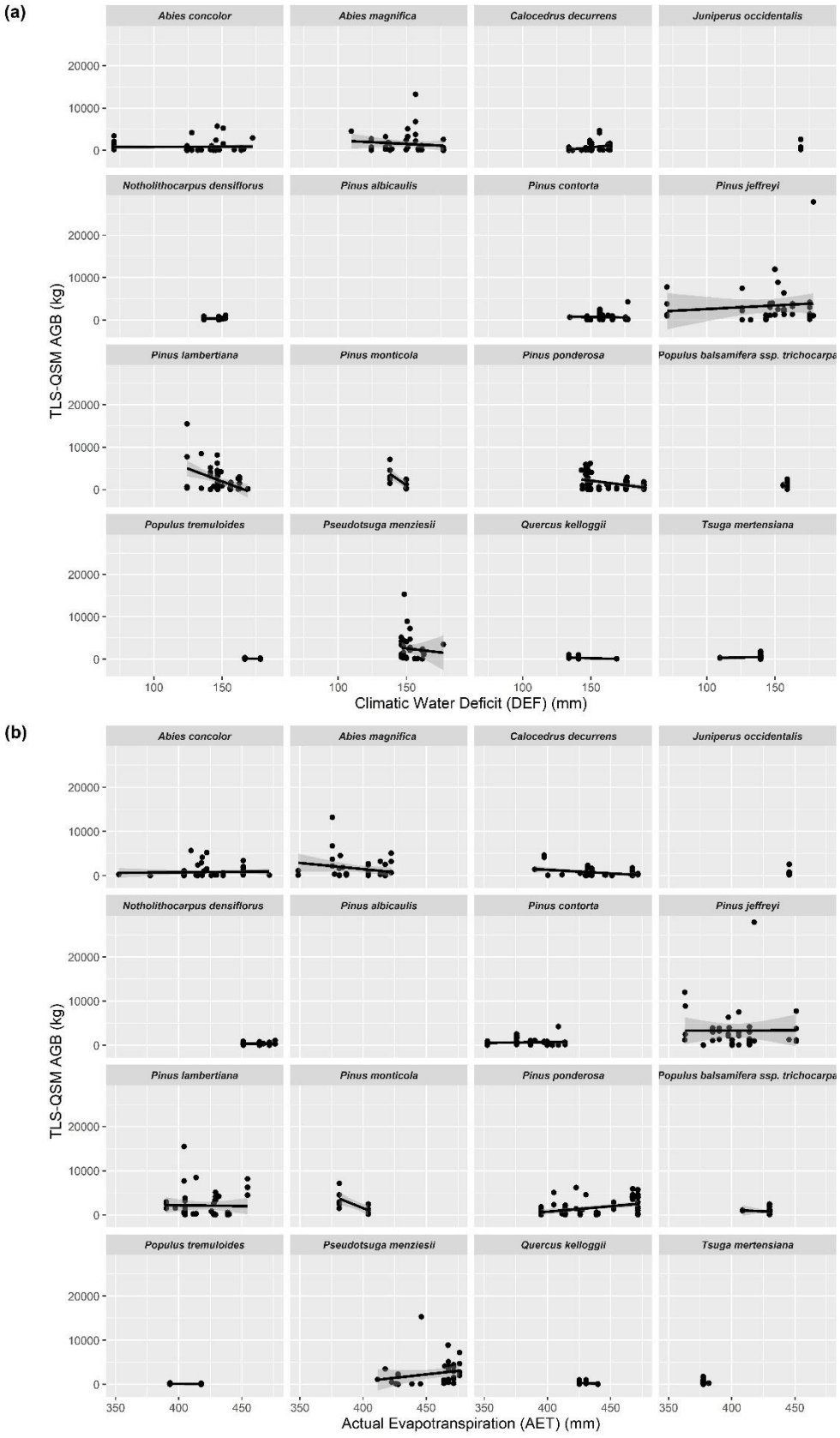
(a)
Abies concolor
Abies magnifica
Calocedrus decurrens
Juniperus occidentalis
Notholithocarpus densiflorus
Pinus albicaulis
Pinus contorta
Pinus jeffreyi
Pinus lambertiana
Pinus monticola
Pinus ponderosa
Populus balsamifera ssp. trichocarpa
Populus tremuloides
Pseudotsuga menziesii
Quercus kelloggii
Tsuga mertensiana
TLS-QSM AGB (kg)
Climatic Water Deficit (DEF) (mm)
(b)
Actual Evapotranspiration (AET) (mm)

Figure 11. Climate variables (DEF and AET) were plotted against AGB (kg) to predict AGB variation across species for a) climatic water deficit and b) annual actual evapotranspiration. There were no consistent trends of a climate effect on AGB across species. *Pinus monticola*, *Pinus lambertiana,* and *Pseudotsuga menziesii* biomass estimate dramatically decreased with increased climatic water deficit.

	Log-Linear Mixed Effect Model					
Predictors	*Estimates*	*std. Error*	*std. Beta*	*standardized std. Error*	*p*	*std. p*
(Intercept)	-2.20	2.60	-0.41	0.07	0.398	**<0.001**
log(def)	-0.01	0.18	0.05	0.04	0.942	0.156
log(aet)	0.11	0.39	0.03	0.03	0.771	0.419
log(DBHqsm_mean.1)	1.66	0.04	0.83	0.04	**<0.001**	**<0.001**
log(Treeheight_mean)	0.71	0.04	0.04	0.04	**<0.001**	0.285
Random Effects						
σ^2	0.08					
$\tau_{00\ Plot}$	0.04					
ICC	0.34					
N_{Plot}	75					
Observations	599					
Marginal R^2 / Conditional R^2	0.954 / 0.969					

Table 7. Non-linear mixed-effects model fitted with log-linear approach predicting the variability of AGB. Tree size (DBH and height) accounted for the majority of the variability within AGB.

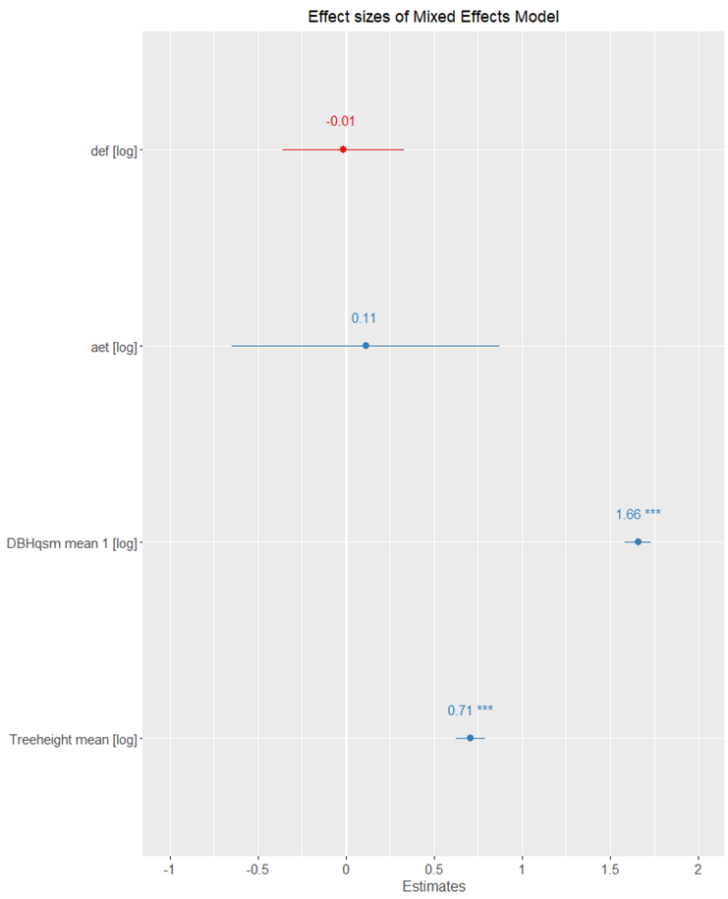

Figure 12. Effect sizes of our predictor variables, DBH, height, DEF, and AET. The climate variables have no effect on the strength or direction of AGB, while DBH was the strongest predictor of AGB variability. As tree size increases, in both girth and height, AGB increases. The blue lines indicate a positive effect on AGB variability and the red lines indicate a negative effect.

4. Discussion

For this study, we evaluated the effectiveness of terrestrial laser scanning (TLS) as a means of creating novel, regional, and species-specific allometric models by reducing biases by increasing sample size across a region and increasing sampling of large and hard to find trees. We compared field measurements against TLS-QSM derived measurements to understand how our models performed against national biomass equations. We created a validation dataset of 75% training data and 25% testing data to

evaluate our TLS allometry on a validation dataset and additionally analyzed the effect of climate on AGB variation.

4.1 Quantitative measurement comparison

We compared TLS-QSM derived DBH with field measured DBH with a linear regression which showed high accuracy with a CCC of 0.98 and RMSE of 4.7 cm (Figure 6). Our results were consistent with studies such as Calders et al. (2015a), Lau et al. (2019), Krause (2021) which accurately recreated DBH from the QSM method. Calders et al. (2015) found a high agreement of TLS-QSM derived DBH (cm) against field-measured DBH, with an RMSE of 2.39 cm, and found that the comparison of TLS-QSM derived volume against destructively harvested trees (n=65) had a low CV(RMSE)=16.1% and a high agreement (CCC=0.98).

Previous studies used destructive data to evaluate the effectiveness of the QSM approach to estimate the AGB of individual trees. Stovall et al. (2018) diameter-height allometric equations showed lower uncertainty than the Jenkins et al. (2003) and Chojnacky et al. (2014) national equations (34.3% and 27.6% respectively) and had an AGB estimation with an RMSE of 20.4 kg and R^2 of 0.98. De Tanago et al. (2019) found TLS allometric models using crown diameter performed slightly better than pantropical models (R^2: 0.87-0.93, CCC: 0.89-0.96) and found that TLS-QSM AGB estimates were not biased, even in cases of irregular trees or trees that were hollow. Lau et al. (2019) found that TLS-QSM derived estimates of AGB of tropical trees in Guyana were not biased and agreed with the reference data.

However, the comparison of TLS-QSM derived height versus field measured height had a higher RMSE of 2.24m, although the correlation fit close to the 1:1 line

(Figure 6). Other studies have seen that TLS-QSM estimates of height agree better with the true values as opposed to field measured height, as seen in Calders et al. (2015). Research has also found that TLS is robust for measuring trees between 15-20m in height with taller trees generally being less accurate when occluded or with decreased visibility (Yang et al. 2019). Field measurements of tree height are sensitive to how dense the forest is, crown size, species, and height (Wang et al. 2019). Calders et al. (2015) found a high agreement of TLS-QSM derived DBH (cm) against field-measured DBH, with an RMSE of 2.39 cm, and found that the comparison of TLS-QSM derived volume against destructively harvested trees (n=65) had a low CV(RMSE)=16.1% and a high agreement (CCC=0.98). However, comparisons of TLS - and field-measured tree heights were found to have large discrepancies, as the field-measured height can lead to large measurement errors due to stand density and crown size (Wang et al. 2019). Calders et al. (2015) found that field- height underestimated trees < 16m tall and overestimate trees > 16 m with an RMSE of 1.28 m, while TLS- derived heights agreed closely with destructively harvested data, with an RMSE of 0.55m.

Other studies have compared biomass estimates from destructive data to TLS-derived biomass to evaluate the effectiveness of the QSM approach to estimate the AGB of individual trees. Stovall et al. (2018) diameter-height allometric equations showed lower uncertainty than the Jenkins et al. (2003) and Chojnacky et al. (2014) national equations (34.3% and 27.6% respectively) and had an AGB estimation with an RMSE of 20.4 kg and R^2 of 0.98. de Tanago et al. (2019) found TLS allometric models using crown diameter performed slightly better than pantropical models (R^2: 0.87-0.93, CCC: 0.89-0.96) and found that TLS-QSM AGB estimates were not biased, even in cases of

irregular trees or trees that were hollow. Lau et al. (2019) found that TLS-QSM derived estimates of AGB of tropical trees in Guyana were not biased and agreed with the reference data.

This quantitative tree metric measurement comparison demonstrates the feasibility of TLS to provide highly accurate tree structure metrics across our AOI and across species. Our stratified random sampling approach means that the target trees are variable in not only size and shape, but variable in the stand condition and location of the target trees sampled. The high accuracy demonstrated by our DBH measurement comparison shows that TLS-QSM is an effective way to recreate tree structure.

4.2 TLS Allometry

Our TLS allometric-DBH models demonstrated high agreement with TLS-QSM AGB (CCC=0.95-0.99) when looking at individual species biomass estimations (Figure 8) for the 10 tree species that had large sample sizes (n >40). This study found that the DBH-only all species model performed better than the DBH-Height all species model. The inclusion of height in our allometric equations did not improve the all species allometric model and reduced the CCC to 0.93 for the DBH-Height model. This may be explained by discrepancies between the largest versus the tallest trees in our dataset. The largest diameter trees in the northern Sierra Nevada do not necessarily equate to the tallest trees, as the tallest tree in our dataset (*Pinus ponderosa*) is 51 meters tall and only 80 cm at DBH. The largest diameter tree in our dataset (178cm), *Pinus jeffreyi*, has a height of 45 meters. However, the inclusion of height improved the allometry by better representing tree structure and reduced the RMSE in both mean and range *Abies concolor, Juniperus occidentalis, Pinus albicaulis, Pinus monticola, Populus*

tremuloides, and *Quercus kelloggii* (Table 5). Some of our low sample size tree species (n=6 and n=14) are rare species that are not commonly found in our AOI and tended to have a lower RMSE (e.g. *Pinus monticola, Pinus albicaulis,* and *Juniperus occidentalis*) but the allometric model did not encompass the range of tree structure variability and the low RMSE values reported are not a reliable representation of allometric model uncertainty. Duncanson et al. (2015) found that small sample sizes lead to an overestimation of biomass at a certain DBH size because the allometric parameters used to create models are very sensitive to sample size. Stovall et al. (2018) found that the low sample size equations had high RMSE if large trees were not included, and we found this was true for our small tree species datasets (*Pinus albicaulis*). Our low sample size species include less common species found in the northern Sierra Nevada and were only found in one or two plots in our TLS dataset. Thus, the reported RMSE for low sample size species may not represent the variability found in that tree species and reinforces the need for further research specifically on the rare and low sample size species. There is room to build on these TLS-derived allometric models by increasing the sample size and increasing the variability of tree size sampled for *Pinus monticola*, *Pinus albicaulis,* and *Juniperus occidentalis*. The higher sample size species-specific equations (n=40 to n=67) likely represented the range of structure and size found in the species but also represented most of the variability found in that species and was a better predictor of biomass when compared to TLS-QSM derived biomass.

One of the goals of this study was to create allometric models that included as many large trees as possible because the regression coefficients observed when large trees are absent are unrealistic when used to predict large-diameter biomass. Large trees

contain approximately 40% of stand-level biomass (Brown, 1997) and including large-diameter trees in our models potentially can drastically improve upon large tree biomass predictions for future use. Stovall et al. (2018) demonstrated that the inclusion of large trees in allometric models reduces prediction bias, and the inclusion of large trees in low sample size equations (n=30 to n=50) reduced RMSE. Due to studies demonstrating that low sample sizes equate to prediction bias and lead to uncertainties in allometric models (Duncanson et al. 2015, Stovall et al. 2018), we aimed to gather high sample sizes across all species in our study area. However, time and species occurrence constraints only allowed us to have high sample sizes for 8 tree species with n > 40. The 10 species with large sample sizes (*Abies concolor, Abies magnifica, Calocedrus decurrens, Pinus contorta, Pinus jeffreyi, Pinus lambertiana, Pinus ponderosa, Populus tremloides, Pseudotsuga menziesii,* and *Tsuga mertensiana*) had the highest allometric DBH^2H model CCCs (0.94-0.99) and lowest relative RMSE (%)(16-28%) values. These results, combined with the high agreement demonstrated in the linear regressions in Figure 8, lend credibility to these TLS-derived nondestructive allometric equations.

One source of error to consider for these allometric models was the inability of this study to compare against destructively harvested tree biomass data. We relied upon the low error (5-15%) reported in previous studies (Hackenberg et al. 2015, Calders et al. 2015, Stovall and Shugart, 2018) and the high agreement of the quantitative measurement comparison of field-measured tree metrics against QSM derived tree metrics to determine the feasibility of our TLS-QSM derived biomass estimates. However, the objective of this study was not to compare against destructively harvested data but to develop novel equations without cutting down trees.

We created region and species-specific allometric models as a novel, non-destructive approach for biomass model creation, but also as applicable biomass models for researchers to utilize in the northern Sierra Nevada. We used a parametric approach to create three allometric models using two easy-to-measure and commonly measured tree metrics, DBH, and height (Figure 7). TLS allometry allows researchers to measure biomass across a region efficiently, effectively, and non-destructively.

4.2 National equation comparison

In the United States, national allometric equations such as Jenkins et al. (2003) and Chojnacky et al. (2014) are commonly used for biomass estimation and are created through a literature meta-analysis which is largely derived from destructively harvested trees. The Jenkins models have been shown to underestimate biomass when compared to TLS allometry and had more uncertainty when compared to TLS allometry (Stovall et al. 2018). Contrary to Stovall et al. (2018), our results suggest that both TLS allometry and TLS-QSM biomass estimates were lower than both the Jenkins and Chojnacky national equations for seven species, e.g. *Abies concolor, Abies magnifica, Calocedrus decurrens, Pinus contorta, Populas basamifera ssp. trichocarpa, Quercus kelloggii* and *Tsuga mertensiana* (Figure 9*).* Our allometric models showed better agreement with the Jenkins et al. (2003) allometric models, with a CCC of 0.96 and an RMSE of 693 kg. We did not apply a correction factor to any of our models with high RMSE, which probably contributed to some species having a high RMSE value compared to national scale models. However, we did not want to add any more unneeded biases to allometric models by using correction factors and chose to leave them out of our approach. While the national scale models deviated from our species-specific models in some species, national

scale models have been shown to not perform well at large diameter sizes and are not representative of the wood specific gravity or tree variability found at the northern Sierra Nevada spatial scale.

4.3 Climate effect

Negative impacts of global climate change have been reported on forests, including changes in carbon sequestration (Fang et al. 2018) and forest biomass (Zhang et al. 2018). Forests in North America function as a carbon sink and absorb a substantial amount of CO_2 from the atmosphere (Pan et al. 2011). Processes affecting a forest's ability to act as a carbon sink include forest recovery brought about by land-use change such as fire suppression, reduced harvesting or agricultural abandonment, and climate change (Houghton, 2003). Studies have found a relationship between climate and aboveground biomass, with climate dictating current distributions of species, and indicate potentially species distribution shifts as climate changes and drought stress increases in the northern Sierra Nevada. We used a log-linear mixed-effects model to analyze the effect of climate on our allometric equations. The results indicated that climate did not influence equation variability on all species (Figure 11). We did not investigate the effect of climate on individual species-specific equations, as it was not a goal of this study to evaluate how each individual equation performed the effect of climate. We found a positive effect of tree size (DBH and height) which accounted for most of the variability of AGB (R^2, 0.97, Table 7 and Figure 12). While our study did not find an effect of climate on AGB variation, the climate, in particular actual evapotranspiration and annual climatic water deficit, are very well correlated with vegetation species distribution (Stephenson, 1998). In order to complete a more comprehensive study of climate and

AGB, we could increase the sample size across our AOI and sample as evenly as possible across arid and wet forests in the northern Sierra Nevada. While this study does not focus on the topoclimate effects on AGB variation, our results provide an interesting insight that climate does not play a role in TLS-derived allometric equation variability across species and across the northern Sierra Nevada region.

4.4 Conclusions

Terrestrial LiDAR allows for highly detailed data collected on tree structure to be derived over large areas and surpasses the capabilities of traditional forestry. We non-destructively 48 created species-specific relationships spanning the northern Sierra Nevada topoclimatic gradient to predict biomass. We included large trees and less common trees that would be illegal, expensive, inconvenient, or unnecessary to destructively harvest in our model creation to better represent tree structure and forest structure of our AOI. Future work can expand on the sample sizes and tree species used here to create larger sample sizes spanning a diverse range of tree sizes to better estimate the biomass of the northern Sierra Nevada forests.

References

Ahmed R, Siqueira P, Hensley S, Bergen K (2013) Uncertainty of Forest Biomass Estimates in North Temperate Forests Due to Allometry: Implications for Remote Sensing. Remote Sensing 5:3007–3036. https://doi.org/10.3390/rs5063007

Anderson-Teixeira KJ, Davies SJ, Bennett AC, et al (2015) CTFS-ForestGEO: a worldwide network monitoring forests in an era of global change. Glob Change Biol 21:528–549. https://doi.org/10.1111/gcb.12712

Anderson-Teixeira KJ, McGarvey JC, Muller-Landau HC, et al (2015) Size-related scaling of tree form and function in a mixed-age forest. Funct Ecol 29:1587–1602. https://doi.org/10.1111/1365-2435.12470

Archibald S, Bond WJ (2003) Growing tall vs growing wide: tree architecture and allometry of *Acacia karroo* in forest, savanna, and arid environments. Oikos 102:3–14. https://doi.org/10.1034/j.1600-0706.2003.12181.x

Baskerville GL (1972) Use of Logarithmic Regression in the Estimation of Plant Biomass. Can J For Res 2:49–53. https://doi.org/10.1139/x72-009

Bates D, Mächler M, Bolker B, Walker S (2015) Fitting Linear Mixed-Effects Models Using lme4. J Stat Soft 67:. https://doi.org/10.18637/jss.v067.i01

Bohlman S, O'Brien S (2006) Allometry, adult stature and regeneration requirement of 65 tree species on Barro Colorado Island, Panama. J Trop Ecol 22:123–136. https://doi.org/10.1017/S0266467405003019

Brown S (1997) Estimating biomass and biomass change of tropical forests: a primer. Food and Agriculture Organization of the United Nations, Rome

Burt A, Disney MI, Armston J, et al (2013) Rapid characterisation of forest structure from TLS and 3D modelling. IEEE. https://doi.org/10.1109/IGARSS.2013.6723555

Calders K, Adams J, Armston J, et al (2020) Terrestrial laser scanning in forest ecology: Expanding the horizon. Remote Sensing of Environment 251:112102. https://doi.org/10.1016/j.rse.2020.112102

Calders K, Newnham G, Burt A, et al (2015) Nondestructive estimates of above-ground biomass using terrestrial laser scanning. Methods Ecol Evol 6:198–208. https://doi.org/10.1111/2041-210X.12301

Chave J, Andalo C, Brown S, et al (2005) Tree allometry and improved estimation of carbon stocks and balance in tropical forests. Oecologia 145:87–99. https://doi.org/10.1007/s00442-005-0100-x

Chave J, Condit R, Aguilar S, et al (2004) Error propagation and scaling for tropical forest biomass estimates. Phil Trans R Soc Lond B 359:409–420. https://doi.org/10.1098/rstb.2003.1425

Chave J, Muller-Landau HC, Baker TR, et al (2006) Regional and phylogenetic variation of wood density across 2456 neotropical tree species. Ecological Applications 16:2356–2367. https://doi.org/10.1890/1051-0761(2006)016[2356:RAPVOW]2.0.CO;2

Chojnacky DC, Heath LS, Jenkins JC (2014) Updated generalized biomass equations for North American tree species. Forestry 87:129–151. https://doi.org/10.1093/forestry/cpt053

Clevers JGPW, Kooistra L, Schaepman ME (2010) Estimating canopy water content using hyperspectral remote sensing data. International Journal of Applied Earth

Observation and Geoinformation 12:119–125. https://doi.org/10.1016/j.jag.2010.01.007

Clifford D, Cressie N, England JR, et al (2013) Correction factors for unbiased, efficient estimation and prediction of biomass from log–log allometric models. Forest Ecology and Management 310:375–381. https://doi.org/10.1016/j.foreco.2013.08.041

Dietze MC, Wolosin MS, Clark JS (2008) Capturing diversity and interspecific variability in allometries: A hierarchical approach. Forest Ecology and Management 256:1939–1948. https://doi.org/10.1016/j.foreco.2008.07.034

Disney M, Burt A, Calders K, et al (2019) Innovations in Ground and Airborne Technologies as Reference and for Training and Validation: Terrestrial Laser Scanning (TLS). Surv Geophys 40:937–958. https://doi.org/10.1007/s10712-019-09527-x

Disney MI, Boni Vicari M, Burt A, et al (2018) Weighing trees with lasers: advances, challenges and opportunities. Interface Focus 8:20170048. https://doi.org/10.1098/rsfs.2017.0048

Duncanson L, Rourke O, Dubayah R (2015) Small Sample Sizes Yield Biased Allometric Equations in Temperate Forests. Sci Rep 5:17153. https://doi.org/10.1038/srep17153

Fang J, Yu G, Liu L, et al (2018) Climate change, human impacts, and carbon sequestration in China. Proc Natl Acad Sci USA 115:4015–4020. https://doi.org/10.1073/pnas.1700304115

Fatemi FR, Yanai RD, Hamburg SP, et al (2011) Allometric equations for young northern hardwoods: the importance of age-specific equations for estimating aboveground biomass. Can J For Res 41:881–891. https://doi.org/10.1139/x10-248

Flewelling JW, Piennar LV (1981) Multiplicative Regression with Lognormal Errors. Forest Science 27:281–289. https://doi.org/https://doi.org/10.1093/forestscience/27.2.281

Fowler HJ, Blenkinsop S, Tebaldi C (2007) Linking climate change modelling to impacts studies: recent advances in downscaling techniques for hydrological modelling: Advances in downscaling techniques for hydrological modelling. Int J Climatol 27:1547–1578. https://doi.org/10.1002/joc.1556

Fox J, Weisberg S (2019). *An R Companion to Applied Regression*, Third edition. Sage, Thousand OakCA. https://socialsciences.mcmaster.ca/jfox/Books/Companion/.

Galik CS, Mobley ML, deB. Richter D (2009) A virtual "field test" of forest management carbon offset protocols: the influence of accounting. Mitig Adapt Strateg Glob Change 14:677–690. https://doi.org/10.1007/s11027-009-9190-9

Girardeau-Montaut, D. (2020). Cloudcompare

Goetz SJ, Baccini A, Laporte NT, et al (2009) Mapping and monitoring carbon stocks with satellite observations: a comparison of methods. Carbon Balance Manage 4:2. https://doi.org/10.1186/1750-0680-4-2

Gonzalez de Tanago J, Lau A, Bartholomeus H, et al (2018) Estimation of above-ground biomass of large tropical trees with terrestrial LiDAR. Methods Ecol Evol 9:223–234. https://doi.org/10.1111/2041-210X.12904

Hackenberg J, Morhart C, Sheppard J, et al (2014) Highly Accurate Tree Models Derived from Terrestrial Laser Scan Data: A Method Description. Forests 5:1069–1105. https://doi.org/10.3390/f5051069

Hartsook T (2021) Discovetree - An Automated Tool To Generate Stem Maps From Terrestrial Laser Scanner Point Clouds. University of Nevada, Reno

Houghton RA (2003) Revised estimates of the annual net flux of carbon to the atmosphere from changes in land use and land management 1850-2000. Tellus B 55:378–390. https://doi.org/10.1034/j.1600-0889.2003.01450.x

Ilic, J., D. Boland, M. Mcdonald, G. Downes and P. Blakemore, 2000. Wood density phase 1: State of knowledge, national carbon accounting system. Australian Greenhouse Office, Commonwealth of Australia. Technical Report No. 18.

Jenkins JC, Chojnacky DC, Heath LS, Birdsey RA (2003) National-Scale Biomass Estimators for United States Tree Species. Forest Science 49:12–35

King DA (1996) Allometry and life history of tropical trees. J Trop Ecol 12:25–44. https://doi.org/10.1017/S0266467400009299

Krause P (2021) Using terrestrial laser scanning to evaluate non-destructive aboveground biomass allometries in diverse Northern California forests. Sonoma State University

Kukko A, Kaasalainen S, Litkey P (2008) Effect of incidence angle on laser scanner intensity and surface data. Appl Opt 47:986. https://doi.org/10.1364/AO.47.000986

Lambert MC, Ung CH, Rauliler F (2005) Canadian national tree aboveground biomass equations. Canadian Journal for Forest Research 35:. https://doi.org/ 10.1139/X05-112

Lau A, Calders K, Bartholomeus H, et al (2019) Tree Biomass Equations from Terrestrial LiDAR: A Case Study in Guyana. Forests 10:527. https://doi.org/10.3390/f10060527

Le Quéré C, Andrew RM, Friedlingstein P, et al (2018a) Global Carbon Budget 2017. Earth Syst Sci Data 10:405–448. https://doi.org/10.5194/essd-10-405-2018

Le Quéré C, Andrew RM, Friedlingstein P, et al (2018b) Global Carbon Budget 2017. Earth Syst Sci Data 10:405–448. https://doi.org/10.5194/essd-10-405-2018

Lutz JA, van Wagtendonk JW, Franklin JF (2010) Climatic water deficit, tree species ranges, and climate change in Yosemite National Park. Journal of Biogeography 37:936–950. https://doi.org/10.1111/j.1365-2699.2009.02268.x

MATLAB. (2010). version 7.10.0 (R2019b). Natick, Massachusetts: The MathWorks Inc.

Mitchard ET, Saatchi SS, Baccini A, et al (2013) Uncertainty in the spatial distribution of tropical forest biomass: a comparison of pan-tropical maps. Carbon Balance Manage 8:10. https://doi.org/10.1186/1750-0680-8-10

Momo Takoudjou S, Ploton P, Sonké B, et al (2018) Using terrestrial laser scanning data to estimate large tropical trees biomass and calibrate allometric models: A comparison with traditional destructive approach. Methods Ecol Evol 9:905–916. https://doi.org/10.1111/2041-210X.12933

Morrison B (2018) POTENTIAL PAST AND FUTURE TREE MIGRATION RESPONSES TO CLIMATE CHANGE. University of Illinois at Urbana-Champaign

Pan Y, Birdsey RA, Fang J, et al (2011a) A Large and Persistent Carbon Sink in the World's Forests. Science 333:988–993. https://doi.org/10.1126/science.1201609

Pan Y, Birdsey RA, Fang J, et al (2011b) A Large and Persistent Carbon Sink in the World's Forests. Science 333:988–993. https://doi.org/10.1126/science.1201609

Pesci A, Giordano T (2008) Effects of surface irregularities on intensity data from laser scanning: an experimental approach. Annals of Geophysics 51:. https://doi.org/10.4401/ag-4462

Picard N, Saint-Andre L, Henry M (2012) Manual for building tree volume and biomass allometric equations: from field measurement to prediction . FAO, Rome, Italie

Pugh TAM, Lindeskog M, Smith B, et al (2019) Role of forest regrowth in global carbon sink dynamics. Proc Natl Acad Sci USA 116:4382–4387. https://doi.org/10.1073/pnas.1810512116

R Core Team (2021). R: A language and environment for statistical computing. R Foundation for Statistical Computing, Vienna, Austria. URL https://www.R-project.org/.

RapidLasso GmbH. (2019). Lastools version 191111.

Raumonen, P. (updated 2020). TreeQSM Quantitative Structure Models of Single Trees from Laser Scanner Data Instructions for MATLAB-software TreeQSM, version 2.4.0

Raumonen P, Casella E, Calders K, et al (2015) MASSIVE-SCALE TREE MODELLING FROM TLS DATA. ISPRS Ann Photogramm Remote Sens Spatial Inf Sci II-3/W4:189–196. https://doi.org/10.5194/isprsannals-II-3-W4-189-2015

Raumonen P, Kaasalainen M, Åkerblom M, et al (2013) Fast Automatic Precision Tree Models from Terrestrial Laser Scanner Data. Remote Sensing 5:491–520. https://doi.org/10.3390/rs5020491

Riegl Laser Measurement Systems GmbH, 2020

Sprugel DG (1983) Correcting for Bias in Log-Transformed Allometric Equations. Ecology 64:209–210. https://doi.org/10.2307/1937343

Stephenson N (1998) Actual evapotranspiration and deficit: biologically meaningful correlates of vegetation distribution across spatial scales. J Biogeography 25:855–870. https://doi.org/10.1046/j.1365-2699.1998.00233.x

Stephenson NL (1990) Climatic Control of Vegetation Distribution: The Role of the Water Balance. The American Naturalist 135:649–670. https://doi.org/10.1086/285067

Stovall AEL, Anderson-Teixeira KJ, Shugart HH (2018) Assessing terrestrial laser scanning for developing non-destructive biomass allometry. Forest Ecology and Management 427:217–229. https://doi.org/10.1016/j.foreco.2018.06.004

Swenson NG, Enquist BJ (2007) Ecological and evolutionary determinants of a key plant functional trait: wood density and its community-wide variation across latitude and elevation. American Journal of Botany 94:451–459. https://doi.org/10.3732/ajb.94.3.451

USDA Forest Service. 1981. *CALVEG: A Classification of California Vegetation*. Pacific Southwest Region, Regional Ecology Group, San Francisco CA. 168 pp.

Wang Y, Lehtomäki M, Liang X, et al (2019) Is field-measured tree height as reliable as believed – A comparison study of tree height estimates from field measurement, airborne laser scanning and terrestrial laser scanning in a boreal forest. ISPRS Journal of Photogrammetry and Remote Sensing 147:132–145. https://doi.org/10.1016/j.isprsjprs.2018.11.008

West BJ, Griffin L (1999) Allometric Control, Inverse Power Laws and Human Gait. Chaos, Solitons & Fractals 10:1519–1527. https://doi.org/10.1016/S0960-0779(98)00149-0

Wilkes P, Disney M, Vicari MB, et al (2018a) Estimating urban above ground biomass with multi-scale LiDAR. Carbon Balance Manage 13:10. https://doi.org/10.1186/s13021-018-0098-0

Wilkes P, Disney M, Vicari MB, et al (2018b) Estimating urban above ground biomass with multi-scale LiDAR. Carbon Balance Manage 13:10. https://doi.org/10.1186/s13021-018-0098-0

Williamson GB, Wiemann MC (2010) Measuring wood specific gravity…Correctly. American Journal of Botany 97:519–524. https://doi.org/10.3732/ajb.0900243

Woodall C, Heath L, Domke G, Nichols M (2010) Methods and equations for estimating aboveground volume, biomass, and carbon for trees in the U.S. forest inventory, 2010. Gen Tech Rep. NRS-88: https://doi.org/https://doi.org/10.2737/NRS-GTR-88.

Yang B, Lee DK, Heo HK, Biging G (2019) The effects of tree characteristics on rainfall interception in urban areas. Landscape Ecol Eng 15:289–296. https://doi.org/10.1007/s11355-019-00383-w

Zhang T, Niinemets Ü, Sheffield J, Lichstein JW (2018) Shifts in tree functional composition amplify the response of forest biomass to climate. Nature 556:99–102. https://doi.org/10.1038/nature26152

Zheng D, Ducey MJ, Heath LS (2013) Assessing net carbon sequestration on urban and community forests of northern New England, USA. Urban Forestry & Urban Greening 12:61–68. https://doi.org/10.1016/j.ufug.2012.10.003

Conclusion

This thesis demonstrated a non-destructive and novel approach that recreates tree structure from terrestrial laser scanning (TLS) data to create biomass estimates of northern Sierra Nevada tree species. This approach improves upon classic allometric methods that use destructive harvesting to obtain the biomass of trees by increasing sample size, increase accessibility, and increasing the range of species and size of trees sampled. Results from this study demonstrate that species with a high sample size ($N > 40$) and species that included large trees (DBH > 70 cm) captured a variability of tree size and form that is not usually represented by classic allometric methods. As traditional allometric approaches for estimating biomass for tree species that have high sample sizes do not significantly differ from TLS estimated biomass (Calders et al. 2015), TLS can offer a new approach for obtaining increasing larger sample sizes to more precisely estimate biomass in a cost-effective way. In addition, TLS data can supplement other remote sensing methods, such as airborne LiDAR biomass estimates, to work towards rapid and large-scale AGB estimations (Silva et al., 2020). TLS derived allometric equations have the potential to use climate and additional remote sensing predictors to estimate biomass, and not just the traditionally used DBH and height.

References

Calders K, Newnham G, Burt A, et al (2015) Nondestructive estimates of above-ground biomass using terrestrial laser scanning. Methods Ecol Evol 6:198–208. https://doi.org/10.1111/2041-210X.12301

Silva CA, Duncanson L, Hancock S, et al (2021) Fusing simulated GEDI, ICESat-2 and NISAR data for regional aboveground biomass mapping. Remote Sensing of Environment 253:112234. https://doi.org/10.1016/j.rse.2020.112234